arXiv:2101.01622v1 [astro-ph.GA] 5 Jan 2021

A Multiwavelength Survey of Wolf-Rayet Nebulae in the Large Magellanic Cloud

Clara Shang Hung （洪宇函）,[1,2] Po-Sheng Ou （歐柏昇）,[1,3] You-Hua Chu （朱有花）,[1,3,4] Robert A. Gruendl,[4] and Chuan-Jui Li （李傳睿）[1]

[1]*Institute of Astronomy and Astrophysics, Academia Sinica, No.1, Sec. 4, Roosevelt Rd., Taipei 10617, Taiwan, R.O.C.*
[2]*Summit Public School: K2, El Cerrito, CA 94530, U.S.A.*
[3]*Department of Physics, National Taiwan University, No.1, Sec. 4, Roosevelt Rd., Taipei 10617, Taiwan, R.O.C.*
[4]*Department of Astronomy, University of Illinois, 1002 West Green Street, Urbana, IL 61801, U.S.A.*

ABSTRACT

Surveys of Wolf-Rayet (WR) stars in the Large Magellanic Cloud (LMC) have yielded a fairly complete catalog of 154 known stars. We have conducted a comprehensive, multiwavelength study of the interstellar/circumstellar environments of WR stars, using the Magellanic Cloud Emission Line Survey (MCELS) images in the Hα, [O III] , and [S II] lines; *Spitzer Space Telescope* 8 and 24 μm images; Blanco 4m Telescope Hα CCD images; and Australian Telescope Compact Array (ATCA) + Parkes Telescope H I data cube of the LMC. We have also examined whether the WR stars are in OB associations, classified the H II environments of WR stars, and used this information to qualitatively assess the WR stars' evolutionary stages. The 30 Dor giant H II region has active star formation and hosts young massive clusters, thus we have made statistical analyses for 30 Dor and the rest of the LMC both separately and altogether. Due to the presence of massive young clusters, the WR population in 30 Dor is quite different from that from elsewhere in the LMC. We find small bubbles (<50 pc diameter) around ∼12% of WR stars in the LMC, most of which are WN stars and not in OB associations. The scarcity of small WR bubbles is discussed. Spectroscopic analyses of abundances are needed to determine whether the small WR bubbles contain interstellar medium or circumstellar medium. Implications of the statistics of interstellar environments and OB associations around WR stars are discussed. Multiwavelength images of each LMC WR star are presented.

Keywords: ISM: bubbles– stars: Wolf–Rayet

1. INTRODUCTION

Wolf-Rayet (WR) stars are often surrounded by beautiful ring-shaped nebulae in Hα images. Since the discovery of the first three WR ring nebulae, NGC 2359, NGC 6888, and S308 (Johnson & Hogg 1965), systematic surveys of WR nebulae have been conducted in our Galaxy (e.g., Chu 1981; Heckathorn et al. 1982; Chu et al. 1983; Miller & Chu 1993; Marston et al. 1994a,b; Stock & Barlow 2010) and the Large Magellanic Cloud (LMC; e.g., Chu & Lasker 1980; Dopita et al. 1994). It is found that ring nebulae around WR stars can have a variety of morphologies and sizes, possibly indicating different formation mechanisms and evolutionary stages. To carry out a comprehensive investigation of ring nebulae around WR stars, it is beneficial to compile a complete inventory of WR stars in a galaxy and use deep nebular line images to search for associated nebulae.

It is difficult to achieve completeness in the catalog of WR stars in our Galaxy because of the heavy extinction along the Galactic plane. Even the distances of the Galactic WR stars were uncertain before the Gaia data became available (Gaia Collaboration et al. 2018). It would thus be difficult to per-

form statistical and quantitative analyses on the WR nebulae in our Galaxy. The LMC, on the other hand, is at a known 50 kpc distance (Pietrzyński et al. 2019) with little internal and foreground extinction; thus, it is possible to achieve a more complete inventory of WR stars and carry out a thorough multiwavelength search for associated nebulae.

An initial search of WR stars in the LMC by Westerlund & Smith (1964) found 58 objects, and subsequent searches have increased the number of known LMC WR stars to 80 by Fehrenbach et al. (1976); 100 by Breysacher (1981); 135 by Breysacher et al. (1999); and more recently 154 by Neugent et al. (2018). The latest LMC WR star catalog is likely fairly complete.

The search for WR nebulae in the LMC began with Chu & Lasker (1980) using photographic plates taken with the 0.61 m Curtis Schmidt Telescope. Later, Dopita et al. (1994) used the Australian National University 2.3 m Telescope with a spectrograph in the imaging mode, as well as an imager, to conduct a deeper survey on WR nebulae. Stock & Barlow (2010) used digitized Hα photographic plates taken with the 1.2 m UK Schmidt Telescope to search for WR nebulae in

the LMC. The former two surveys used Hα and [O III] images, while the latter used only Hα images. Meanwhile, the Magellanic Cloud Emission Line Survey (MCELS) has been conducted with the Curtis Schmidt Telescope and a CCD camera, providing Hα, [O III], and [S II] images for the entire LMC (Smith, & MCELS Team 1999); furthermore, the *Spitzer Space Telescope* has surveyed the LMC (Meixner et al. 2006) in infrared passbands, and the Australian Telescope Compact Array (ATCA) has surveyed the H I in the LMC with high resolution (Kim et al. 2003). Using these new surveys of neutral and ionized gas and the nearly complete catalog of WR stars in the LMC, we are able to, for the first time, probe the multiphase interstellar environment of WR stars and investigate interactions between the stars and their ambient medium.

This paper reports our survey and analysis of WR nebulae in the LMC. Section 2 expands upon the expected coevolution of a WR star and its environment, Section 3 describes the data and methodology used to conduct this investigation, Section 4 presents the results, Section 5 discusses the implications of our results, and Section 6 summarizes this work.

2. COEVOLUTION OF WR STARS AND THEIR AMBIENT MEDIUM

When WR nebulae were first discovered, neither the evolutionary history of WR stars nor the formation mechanisms of the nebulae were clearly understood. Over the years, stellar evolution models have shown that WR stars are just evolved massive stars, of which some are well beyond the main sequence (MS) and some are still burning hydrogen (Langer 2012). The massive stars' winds during different evolutionary stages have become better known. Hydrodynamic simulations of interactions between massive stars' winds and their ambient medium have been made (e.g., Garcia-Segura et al. 1996a,b), and their results can be used to guide our search for WR nebulae. In this section, we first summarize our early perception of WR nebulae based on data with inadequate resolutions and our incomplete knowledge of stellar evolution and stellar wind interaction. The misunderstandings should be superseded by our current understanding based on numerical simulations made with improved knowledge of stellar evolution and its associated stellar wind properties.

2.1. *Previous Perception*

WR stars are massive stars characterized by broad emission lines in their spectra, indicating the presence of fast stellar winds. Among massive stars, WR stars' winds have the highest mechanical luminosities. The powerful WR winds sweep up the ambient medium to form shell structures that appear as "arcs" or "rings" in Hα images and are called "ring nebulae."

WR nebula surveys used only morphological information in Hα images to identify ring nebulae. More often than not, a WR star is projected near a curved nebular filament, and the physical relationship between the WR star and the nebular feature is tantalizing but not confidently established. Despite the uncertainty, such objects were still identified as WR ring nebulae. Sometimes, a round H II region with a WR star in its central region is also identified as a ring nebula. Thus, WR nebulae became a heterogeneous class of objects.

To investigate the nature of WR ring nebulae, Chu (1981) incorporated internal kinematic properties of the WR nebulae and classified WR ring nebulae into three categories, based on the kinematics and morphologies of the nebulae:

- W-type nebulae are wind-blown bubbles whose dynamic ages are smaller than the lifetime of a WR phase to ensure that the WR winds are responsible for the formation of the bubbles. Such a ring nebula shows a fine filamentary shell around the central star, which is usually projected near the center or toward the brightest part of the nebula.

- E-type nebulae consist of stellar ejecta. The E-type nebulae were introduced to have chaotic and irregular expansions and clumpy morphologies. However, it was later realized that the chaotic expansion reported for M1-67 and RCW 58 (Chu & Treffers 1981; Chu 1982a) was an artifact caused by the large entrance apertures of the Fabry-Perot scanning observations, whereas long-slit high-dispersion spectra actually show uniform expansion pattern despite the large density fluctuations (Solf & Carsenty 1982; Chu 1988). Chemical abundance observations of the E-type WR nebulae show enrichment of nitrogen (e.g., Esteban et al. 1991), confirming that they consist of ejected stellar material, which is called circumstellar medium (CSM).

- R-type nebulae are characterized as "radiatively excited H II regions," consisting of interstellar medium (ISM). R_a denotes amorphous H II regions, while R_s denotes shell nebulae whose dynamic ages are much larger than the lifetime of the WR phase.

When deeper and higher-resolution images are available, it becomes clear that the above classification is too primitive. A more sophisticated approach is needed. The perception of WR nebulae in this subsection should be superseded by the understanding outlined in the next subsection.

2.2. *Current Understanding*

The current knowledge of WR nebulae derives from a better understanding of stellar evolution. We now know that WR stars evolve from MS O stars through either the luminous blue variable (LBV) or red supergiant (RSG) phase (Langer 2012). Garcia-Segura et al. (1996a,b) showed for the first

time a hydrodynamic model of the gaseous environment co-evolving with the central star from the MS phase to the WR phase. Similar hydrodynamic calculations have been carried out by Dwarkadas (2007), Toalá & Arthur (2011), and van Marle & Keppens (2012), all of which have produced qualitatively similar results, as described below.

The WR stars that evolve from the MS through the LBV phase are the most massive, e.g., $\gtrsim 60\ M_\odot$, while those that evolve from MS via the RSG phase are less massive, e.g., $\sim 35\ M_\odot$. In the MS phase, massive stars lose mass at rates of $\sim 10^{-6}\ M_\odot$ yr^{-1} in the form of fast stellar winds with terminal velocities of $\sim$2000–3000 km s^{-1} (Prinja et al. 1990; Puls et al. 1996). During this stage, the MS stellar wind sweeps up the ambient ISM to form an interstellar bubble (Weaver et al. 1977). As a massive star evolves off the MS and into the LBV or RSG phase, the mass loss takes place in the form of copious slow winds, of which the wind velocities are $\sim$10–50 km s^{-1} and mass-loss rates $\sim 10^{-4}\ M_\odot$ yr^{-1} (van Loon et al. 2005). The stellar material lost in this wind expands slowly away from the star, forming a small circumstellar nebula (consisting of CSM) inside the cavity of the interstellar bubble formed previously when the star was in the MS stage.

When the star enters a WR phase, the stellar wind velocity and mass-loss rate increase considerably, with terminal velocities of $\sim$1000–3000 km s^{-1} and mass-loss rates of $\sim 10^{-5}\ M_\odot$ yr^{-1} (Nugis & Lamers 2000). This fast WR wind sweeps up the slowly expanding CSM into a shell, called a circumstellar bubble. Therefore, we expect to see a nested shell structure consisting of a small circumstellar bubble within a larger interstellar bubble around the WR star.

If a WR star has a high velocity with respect to the ambient ISM, either ejected from a cluster or kicked by the supernova explosion of a binary companion, it is a runaway star. For a WR star moving in the ISM, an interstellar bow shock will form in the direction of the star's trajectory. However, if a WR star is surrounded by CSM, which travels together with the WR star, a circumstellar bubble can still form, but the leading edge will be compressed by the ISM and become sharper, denser, and brighter, as seen in the circumstellar bubble around the LBV star S119 (Danforth & Chu 2001).

We have also come to understand that whether a WR star is an isolated single star or located in a cluster environment as a member of an OB association affects the evolution of shell nebulae around the WR star. In the presence of other massive stars, the stellar winds and supernova explosions from all stars collectively form a large shell, called a superbubble (McCray & Kafatos 1987). The formation of a circumstellar WR bubble inside a superbubble is trickier than inside a small interstellar bubble because of possible impacts of stellar winds and supernova explosions from neighboring massive stars.

The largest interstellar structures in a galaxy are supergiant shells (SGSs) whose sizes can approach 1000 pc. The formation of such large shells require multiple generations of star formation to provide the energy. If a WR star is in the low-density interior of an SGS, it may not have a detectable interstellar bubble, although its circumstellar bubble should still be present.

With the known characteristics of the different stages in the evolution of WR stars, we expect to see circumstellar bubbles, interstellar bubbles, superbubbles, and SGSs around WR stars. However, to discern between circumstellar bubbles and interstellar bubbles, observations of nebular abundances are needed, but they are not available to us. Thus, we can only use morphological information to search for small bubbles centered on individual WR stars, superbubbles around WR stars and their host OB associations, and SGSs on the largest scales.

3. DATA AND METHODOLOGY

We have used multiwavelength images to examine the ionized and neutral gaseous environments of the LMC WR stars. We used optical emission-line images to examine the distribution and excitation of ionized gas, the H I 21 cm line data cube to investigate the distribution and kinematics of neutral atomic gas, 8 μm images to identify the partially dissociated regions, and 24 μm images to locate emission from heated dust.

3.1. *Data Used*

MCELS1 is an emission-line survey of the Magellanic Clouds (Smith, & MCELS Team 1999). The survey used the Curtis Schmidt Telescope at Cerro Tololo Inter-American Observatory (CTIO) and a CCD camera to take images in the Hα, [O III] λ5007, and [S II] $\lambda\lambda$6716, 6731 bands, as well as two continuum bands centered at λ6850 and λ5130. In this paper, we only used the emission-line images without continuum subtraction. The Hα images show the overall distribution of ionized gas; the [O III] images, compared with the Hα images, reveal the excitation of ionized gas; and the [S II] images diagnose shocks and ionization fronts.

A higher-resolution Hα survey of the Magellanic Clouds has been conducted with the MOSAIC II camera on the Blanco 4m Telescope at CTIO; this survey has been called MCELS2 (PI: You-Hua Chu). The MOSAIC II camera, which is a mosaic of eight SITe 4096 $\times$ 2048 CCDs, has a pixel size of 0.''27 $\times$ 0.''27 and a field-of-view of 36$'$ $\times$ 36$'$. An Hα filter with 80 Å width was used to record images. In celebration of the 30-year anniversary of the Hubble Space Telescope (HST), a public release of HST Hα image of NGC 2020 became available, and this image is used for WR 71.

The H I data cube was constructed by Kim et al. (2003) using the ATCA survey data in conjunction with single-dish

observations from the Parkes Telescope. This data cube covers $11.1° \times 12.4°$ of the sky with an angular resolution of $1'.0$ and a pixel size of $20''$. The heliocentric velocity coverage, -33 to $+627$ km s^{-1}, is centered at ~300 km s^{-1}, the bulk radial velocity of the LMC. We use the zeroth moment map to present the H I column densities and position-velocity plots to show the kinematic structures of H I gas.

The *Spitzer Space Telescope* Infrared Array Camera (IRAC; Fazio et al. 2004) 8 μm images are used to identify polycyclic aromatic hydrocarbons (PAHs) associated with partially dissociated regions, and the Multiband Imaging Photometer for Spitzer (MIPS; Rieke et al. 2004) 24 μm images to reveal emission from heated dust. The *Spitzer* images of the LMC were from the Legacy Program Surveying the Agents of a Galaxy's Evolution (SAGE; Meixner et al. 2006).

3.2. *Methodology*

We have used our understanding of the coevolution of WR stars in their ambient medium, as detailed in Section 2.2, to guide our search for nebular shells around WR stars. More specifically, to identify wind-blown bubbles, we search for small shells less than ~50 pc in diameter with the WR star in a preferred location indicating that wind-ISM/CSM interaction is responsible for forming the shell. For example, the WR star should be either near the center of a uniform shell or closer to the brighter part of a nonuniform shell; if the structure is a bow-shock-like arc, then the WR star should be near the arc's center of curvature. We identify superbubbles by their large shell sizes, much larger than 50 pc in diameter, or by a central cluster or OB association. For example, the shell around the R136 cluster measures 37.5 pc $\times$ 21 pc in size yet we denote it as a superbubble because of its prominent central cluster. On still a larger scale, we identify SGSs that are greater than ~500 pc in diameter to contextualize the extended star formation history in the WR star's large-scale environment.

To search for nebular shells around WR stars, we first examined the MCELS1 Hα images to obtain a census of ionized gas around the WR stars. We noted the nebular morphology, specifically filaments, arcs, and shell structure in the vicinity of the star. We measured and recorded the dimensions of shell-like features centered on or surrounding the star. In cases where there were no shells, we also noted any emission nebulae around the star. We further used MCELS2 Hα images for a high-resolution view of the filamentary structures in the WR nebula.

To corroborate our findings on the WR nebulae from the Hα images, we examined MCELS1 [O III] and [S II] images to gain insight into the nebular excitation and physical conditions. For early WR stars, i.e., high stellar effective temperatures, we expect to see high [O III] $\lambda5007$/Hα ratios; thus,

bubbles of stars with early spectral types stand out against the ambient medium in the [O III] images better than in the Hα images. Conversely, for late WR stars, the [O III] $\lambda5007$/Hα ratios are low, and the nebulae are usually not detected in [O III] images.

Beyond examining optical images of ionized gas around WR stars, we also extracted the H I zeroth moment map and position-velocity plots for north-south and east-west strips of $20''$ width in order to show the H I column density distribution and the kinematics of the H I gas, respectively. A low-intensity region in the zeroth moment map indicates a depression in the H I column density. A bow-shaped velocity split in a position-velocity plot implies an expanding shell structure.

The dust emissions highlighted by *Spitzer*'s IRAC 8 μm and MIPS 24 μm images were used to gain a more comprehensive understanding of the physical conditions of the WR star's interstellar and circumstellar environments. Some very late-type WR stars with dusty envelopes are also very bright in the 24 μm band.

To see whether a WR star is a member of an OB association (Lucke & Hodge 1970), we compared the WR star's location with the boundaries of OB associations provided in the finding charts in P. Lucke's Ph.D. thesis. WR stars not within the boundaries of an OB association but are within 100 pc to an OB association are also noted, with single parentheses for within 50 pc and double parentheses for 50–100 pc from the center of the OB association. Our results are more quantitative and complete than the compilation by Neugent et al. (2018), who have missed a few associations, such as WR 38 and 39 in LH45, WR 43 in LH 50, WR 53 in LH 62, and WR 55 in LH 61. We record this information in case the WR star is a runaway star from the OB association.

We also identify the H II regions around the WR stars in the Davies et al. (1976) and Henize (1956) H II region catalogs. We further classify their H II regions in three morphological classes. Class 1 refers to a bright, amorphous H II region without filamentary or shell structures. Class 2 indicates that the H II region has a large shell structure, e.g., a superbubble, and it is further divided into two subclasses, with 2a referring to a highly nonuniform shell with the ionizing stars/cluster closer to the brightest rim of the shell and 2b referring to a relatively uniform shell around the ionizing stars/cluster. Lastly, Class 3 indicates a very low-density environment of the WR star. It is further divided into three subclasses: with 3a indicating faint but detectable diffuse emission in the vicinity of the star, 3b indicating the low-density interior of a large shell, and 3c reflecting no detectable diffuse emission in a large-scale diffuse field.

4. RESULTS

Fig. Set 2. LMC WR stars
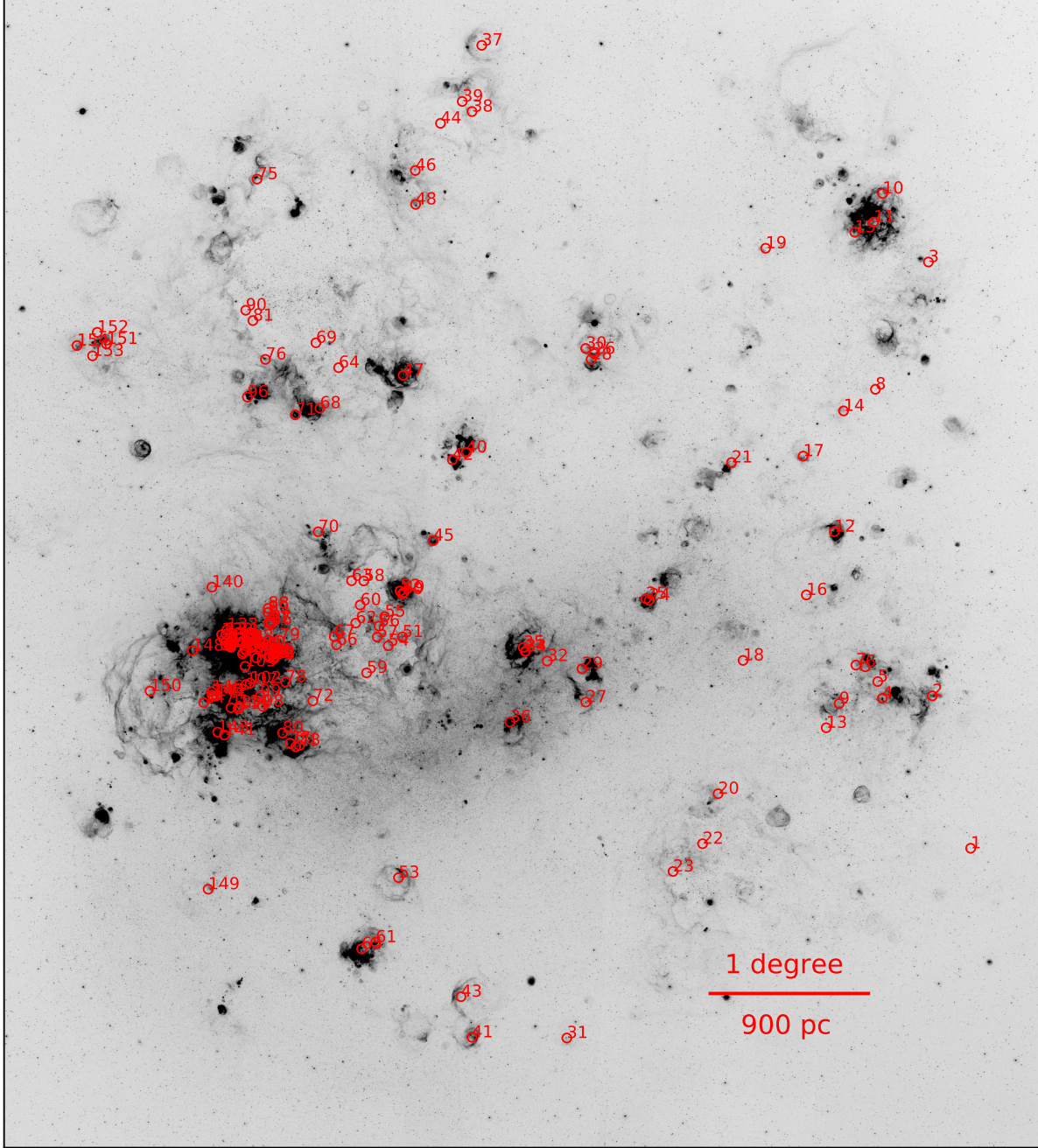
Figure 1. The positions of all the 154 WR stars in the LMC. The running numbers are from Neugent et al. (2018).

The 154 WR stars from Neugent et al. (2018) are marked on the MCELS1 Hα image of the LMC in Figure 1. For each WR star or a close group of WR stars, we make a figure that includes the MCELS2 Hα image; MCELS1 Hα, [O III], and [S II] images; *Spitzer* 8 and 24 μm images; and H I ze-roth moment map and position-velocity plots. An example is shown in Figure 2, and the rest in Fig. Set 2, LMC WR stars. The complete descriptions of individual WR stars and their environments are provided in the Appendix.

We summarize our findings on the stellar and interstellar environments of all 154 WR stars in the LMC in Table 1. Column 1 is the running number of the WR star in Neugent et al. (2018); columns 2 and 3 are the R.A. and decl. of the WR star; columns 4 and 5 are the running numbers of the WR star from Breysacher et al. (1999) and Breysacher (1981), respectively; column 6 is the spectral type of the WR star from Neugent et al. (2018); and column 7 is the host OB association from Lucke & Hodge (1970), where single parentheses mark
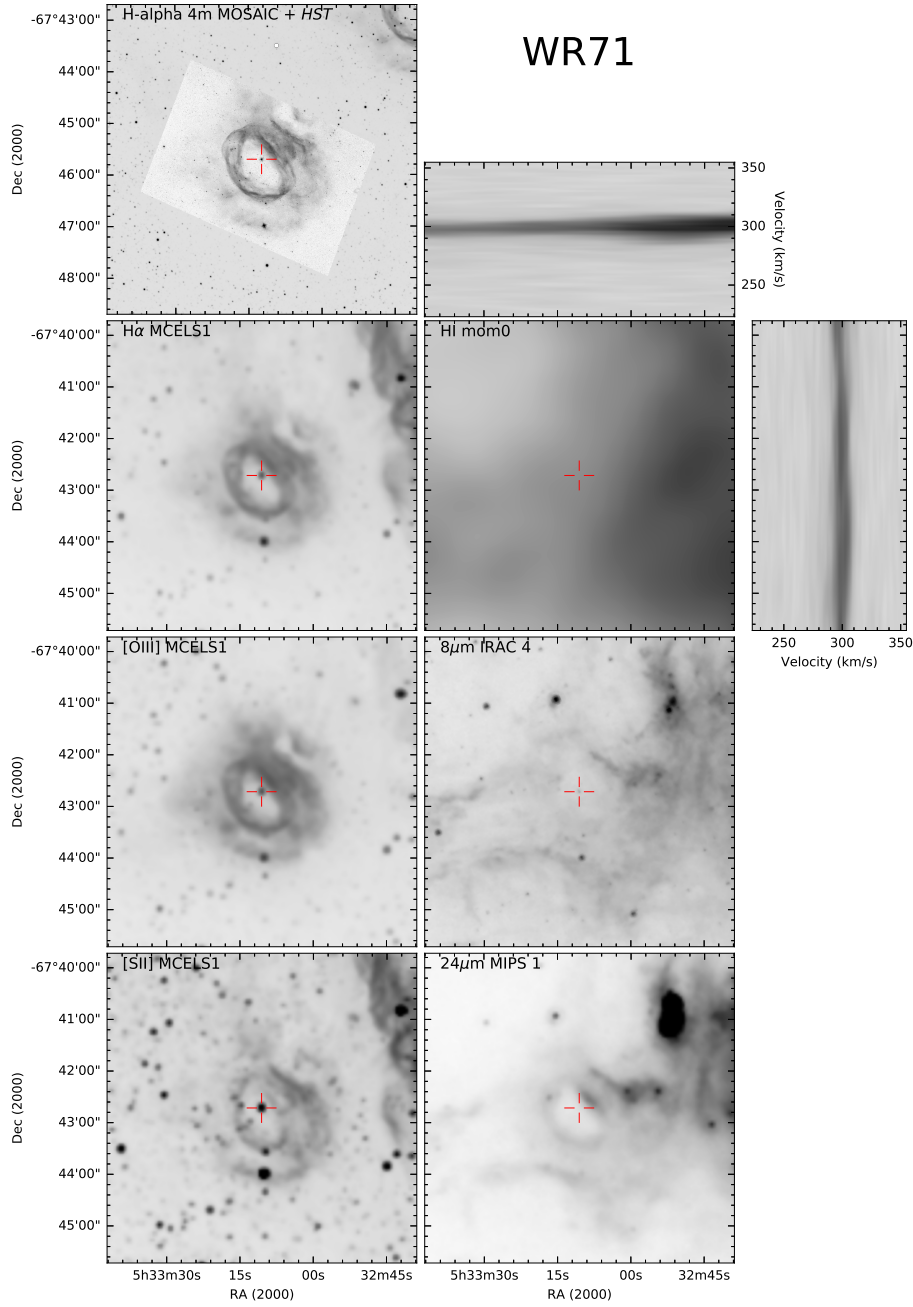
Figure 2. Multiwavelength images of WR stars in the LMC. Each figure has the WR star name (or names) labeled on the top and position marked by a red cross or circle. The origin and passband information is marked on the upper-left corner of each panel. The H I position-velocity plots along the EW and NS directions are plotted above and to the right of the zeroth moment map respectively. The figure of WR 71 is shown here as an example. The complete figure set (99 figures) is available in the online journal.

WR stars not in the OB association but are within 50 pc and double parentheses denote WR stars beyond 50 pc but within 100 pc to the center. Columns 8 and 9 are the associated H II regions from the Henize (1956) and Davies et al. (1976) catalogs; column 10 is the H II morphology classification; columns 11 and 12 are the dimensions of any bubble and superbubble associated with the WR star, respectively; column 13 lists the H II supergiant shells from Meaburn (1980); and column 14 lists the H I giant and supergiant shells from Kim et al. (1999). Note that the use of single parentheses around the H II morphology and bubble/superbubble sizes indicate uncertainty.

In the statistical analysis of WR stars and their associated nebular environments, the 30 Doradus (30 Dor) region needs special consideration because of its extreme properties. 30 Dor is an archetypical giant H II region where star formation is characterized as "starburst" and internal gas dynamics is violent. Early low-resolution radio images of 30 Dor show three peaks in 30 Dor (Le Marne 1968): the brightest peak, 30 Dor A (N157A), corresponds to roughly the 100 pc radius region centered on the R136 cluster, or OB association LH 100; the second brightest peak, 30 Dor B (N157B), corresponds to the H II region around LH 99 and contains a supernova remnant with a pulsar wind nebula (Wang et al. 2001); and the third peak, 30 Dor C (N157C), corresponds to the superbubble around LH 90. These three components are encompassed in DEM L263 (Davies et al. 1976) or N157 (Henize 1956), and within this region exist 43 known WR stars, almost 30% of the whole WR population in the LMC. In the following statistical analyses, we will treat 30 Dor and the rest of the LMC separately, as well as together for the entire LMC. These results will be compared and discussed in the next section.

Of all the variously sized shells encompassing the WR stars, small bubbles are the most relevant to each individual star as the WR wind may be directly responsible for forming the bubble. Thus, we have compiled all small bubbles from Table 1 into Table 2 to examine the statistics of the bubble sizes and WR spectral types. The small bubble around WR 97 in 30 Dor is listed in Table 2 but separated by a horizontal line at the bottom. The Hα images of the 18 small bubbles are shown in Figure 3. We have compiled all superbubbles outside and inside 30 Dor from Table 1 into Tables 3 and 4, respectively, to probe the relationship between WR stars, OB associations, and superbubbles. Images of example superbubbles are shown in Figure 4.

As a reference for the tendency of WR stars' locations in OB associations, we have compiled in Table 5 numbers of WR stars for different spectral types and for the entire LMC, the LMC excluding 30 Dor, and 30 Dor, respectively. To obtain the statistical significance, we combine spectral types into subgroups: WN2-4 (early WN), WN5-6 (mid WN),

WN7-L (late WN), WC4, WC5-6, WO3-4, and "other" for the small number of remaining objects. The LMC WR star catalog of Neugent et al. (2018) has 154 entries, but two entries contain double WR stars and thus the total number of stars in Table 5 is 156. The percentage of WR stars that are in LH OB associations is given in parentheses after the numbers of WR stars in OB associations. It is quite clear that the WR population in the LMC is dominated by WN stars, ∼80%, inside or ouside 30 Dor alike. Within the WN population, there exist more early-type than late-type objects for the entire LMC; however, the WN population differs significantly inside and outside 30 Dor. While outside 30 Dor 73% of WN stars are of WN2-4 types and 9% are WN5-6, inside 30 Dor, only 19% of WN stars are WN2-4 and 62% are WN5-6. Overall, ∼50% of the WR stars are in OB associations; however, WN5-6 and WC stars are more likely to be in OB associations than WN2-4 and WN7-L. Outside 30 Dor, WC stars have the highest percentage to be in OB associations, while inside 30 Dor, WN5-6 stars have the highest percentage to be in OB associations.

Table 6 presents the statistics of the WR star population in the LMC and the fraction of each spectral type with bubbles/superbubbles. In this table, column 1 gives the spectral type grouping, column 2 presents the number (and percentage) of WR stars with bubbles, column 3 presents the number of WR stars with bubbles in OB associations, column 4 presents the number (and percentage) of WR stars in superbubbles, and column 5 presents the number of WR stars with superbubbles in OB associations for all WR stars in the LMC; columns 6-9 present the same information as columns 2-5 for all WR stars in the LMC excluding 30 Dor, respectively; column 10 presents the number (and percentage) of WR stars in superbubbles in 30 Dor and column 11 presents the number of 30 Dor WR stars in superbubbles in OB associations.

In 30 Dor, few small bubbles are identified: WR 97 is surrounded by a small bubble-like structure, while WR 118/119/120 are projected on the southern rim of a triangular shell structure that could be connected to the central superbubble around the R136 cluster, and thus, the bubble nature of the triangular shell is highly uncertain. Several large shell structures in 30 Dor can be identified as superbubbles (Chu & Kennicutt 1994), and WR stars projected within superbubbles in 30 Dor are compiled in Table 4, along with the dimensions of the superbubble and host OB associations. Owing to the scarcity of small WR bubbles in 30 Dor, we only give statistics of WR stars in superbubbles in 30 Dor in Table 6.

We define the H II morphology classes to represent the evolutionary stages of the ISM surrounding the WR stars. Thus, the correlation between the spectral types and the H II morphology classes may be used to diagnose the WR star's progression in its evolution. We have tallied the numbers of WR stars for different spectral types in H II regions of different

morphological classes in Table 7. The results are reported separately for 30 Dor and the LMC excluding 30 Dor, as well as the entire LMC.

5. DISCUSSION

Below we first examine the WR star population in the LMC, using their stellar and interstellar environments to assess their properties, then correlate their bubbles and superbubbles with their spectral types to further probe the nature of the WR spectral types. Finally, we note the impact of WR nebulae on the supernova remnants that are formed after the supernova explosions.

5.1. *WR Star Population in the LMC*
5.1.1. *30 Dor versus the Rest of the LMC*

The distribution of WR stars in the LMC is by no means uniform. Most conspicuously, about 30% of the WR stars in the LMC are concentrated in the 30 Dor giant H II region. As shown in Table 5, the largest difference in the WR star population inside 30 Dor and outside 30 Dor is in the number ratio of WN2-4 to WN5-6 stars, roughly 1:3 in 30 Dor and 8:1 in the rest of the LMC. This reversal in the number ratio of WN2-4 to WN5-6 stars is caused by 30 Dor's young age and massive clusters, where the most massive bins of the initial mass function can be stochastically populated. The evolution of massive stars has been reviewed by Langer (2012), whose Figure 10 shows that the most massive stars evolve into late-type WN stars even during the core hydrogen-burning stage. The large number of WN5-6 stars in 30 Dor coexist with the numerous very massive O2-3 stars (Crowther et al. 2010, 2016), highly suggestive that these WN stars are very massive hydrogen-burning stars, which have been shown to be very luminous and still have hydrogen on their surface (de Koter et al. 1997; Massey & Hunter 1998).

5.1.2. *WR Stars and OB Associations*

The starburst in 30 Dor has produced massive star clusters or OB associations, namely, LH 100 (R136 cluster) in 30 Dor A (Hunter et al. 1995; Massey & Hunter 1998), LH 99 in 30 Dor B (Chu 1997), and LH 90 in 30 Dor C (Lortet & Testor 1984; Testor et al. 1993). It is thus not surprising that 70% of the WR stars in 30 Dor are in OB associations. Among different types of WR stars in 30 Dor, WN5-6 has a higher percentage of being in OB associations than WN2-4, WN7-L, and WC. The R136 cluster is mostly responsible for this high percentage of WN5-6 stars in OB associations in 30 Dor, and these WN5-6 stars are most likely massive hydrogen-burning stars.

In contrast, only 45% of WR stars outside 30 Dor are in OB associations (see Table 5). Interestingly, about 87% of the WC stars outside 30 Dor are in OB associations. In 30 Dor, four out of seven WC stars are in OB associations, corresponding to 57%; however, this is small number statistics.

Furthermore, two WC stars in 30 Dor are within 50 pc from OB associations and could be associated; thus, we do not think the percentage of WC stars in OB associations differs much between 30 Dor and outside 30 Dor.

5.1.3. *WR Stars and Surrounding Ionized ISM*

Massive stars inject energy into the ambient ISM via UV radiation and fast stellar winds during their lifetime and supernova explosions at the end. The energy feedback is expected to produce an amorphous H II region when the massive stars are very young. Gradually, the fast stellar winds of massive stars sweep up the H II region into a shell structure called a bubble (for an isolated massive star) or superbubble (for OB association). Eventually, the shell structure dissipates into the ISM, leaving behind a low-density ISM. These three stages correspond to the three morphological classes of H II environments defined in Section 3.2, with class 1 being the youngest and class 3 being the most evolved stage.

Table 7 shows that in 30 Dor, 15% (7/46) of WR stars are superposed on dense ionized gas (class 1), over 72% (33/46) of WR stars are associated with superbubbles or shell-like structures (class 2), and 13% (6/46) of WR stars in the outskirts of 30 Dor are superposed on diffuse nebulosity with low surface brightness (class 3). Among the 33 WR stars in class 2 H II regions, 29 are inside superbubbles, 3 are projected on the southern rim of the superbubble Shell 5, and 1 is inside a faint shell structure. Twenty-eight of the 29 WR stars in superbubbles are in the two major OB associations (LH 90 and LH 100) that are both surrounded by superbubbles.

Outside 30 Dor, 5% (6/110) WR stars are associated with H II class 1, 36% (40/110) are in superbubbles, and 58% (64/110) are in a very tenuous medium with density lower than 1 H-atom cm^{-3}. It is interesting to note that WN2-4 and WN7-L have the highest percentages associated with H II class 3, the most evolved state. Based on the massive star evolution summarized in Figure 10 of Langer (2012), we suggest that these WN2-4 stars in a very tenuous medium have progenitors with 20–30 $M_\odot$ initial masses, and that these WN7-L stars are the massive helium-burning ones whose progenitors have $\geq 50 M_\odot$ initial masses. Note, however, that this conclusion can change if stellar rotation, close binary evolution, and magnetic fields are considered in models of massive star evolution (Meynet et al. 2017).

5.2. *WR Bubbles: Observation versus Expectation*
5.2.1. *Too Few WR Bubbles are Detected*

According to our current understanding of nebulae around WR stars, as detailed in Section 2.2, we may expect every WR star to be surrounded by a small circumstellar bubble and enclosed by a larger interstellar bubble. However, only six WR stars (WR 2, 4, 17, 52, 61, 154) are inside nested
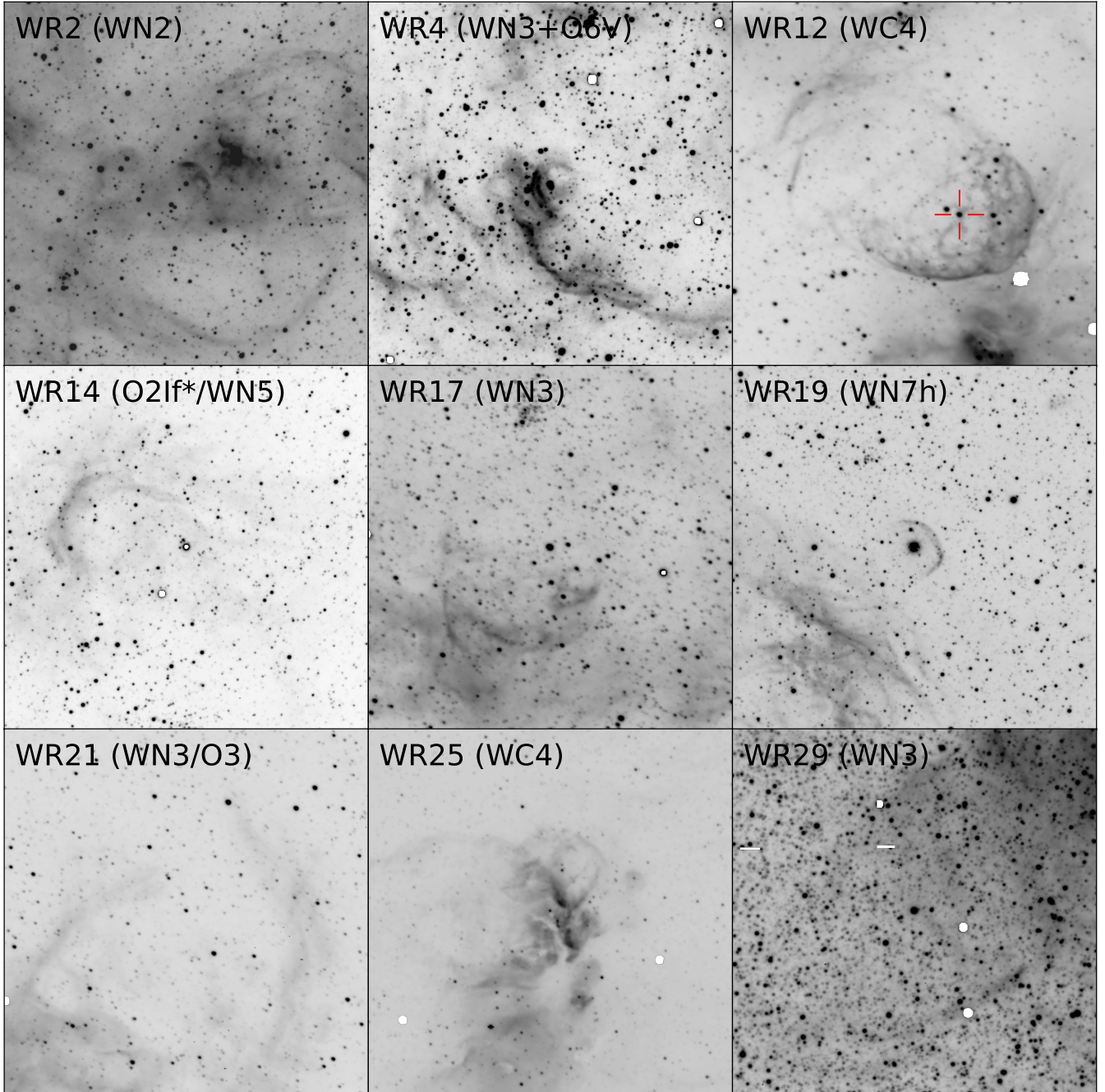
Figure 3. 4m MOSAIC Hα images of small bubbles around WR stars in the LMC. The field of view of each panel is 4'×4'. The WR star is at the center of the panel except WR 12, which is marked by a red cross.

small and large shells, which could be candidates for circumstellar and interstellar bubbles. In fact, only 12% of WR stars are surrounded by small bubbles and only a small fraction of these bubbles have abundance observations to confirm that they are in fact circumstellar bubbles.

The scarcity of small bubbles observed around WR stars needs explanation. It is possible that a close binary companion may perturb and redirect the mass outflow of the WR star's progenitor, prohibiting the formation of a circumstellar bubble. However, ∼24% of LMC WR stars with small bubbles are binary, and among all LMC WR stars, ∼22% are binary, not too different from that for WR stars with small bubbles, suggesting that binarity may not be a main factor in prohibiting the formation of circumstellar bubbles.

A more plausible cause for the nondetection of circumstellar bubbles may be in its evolution. It is conceivable that
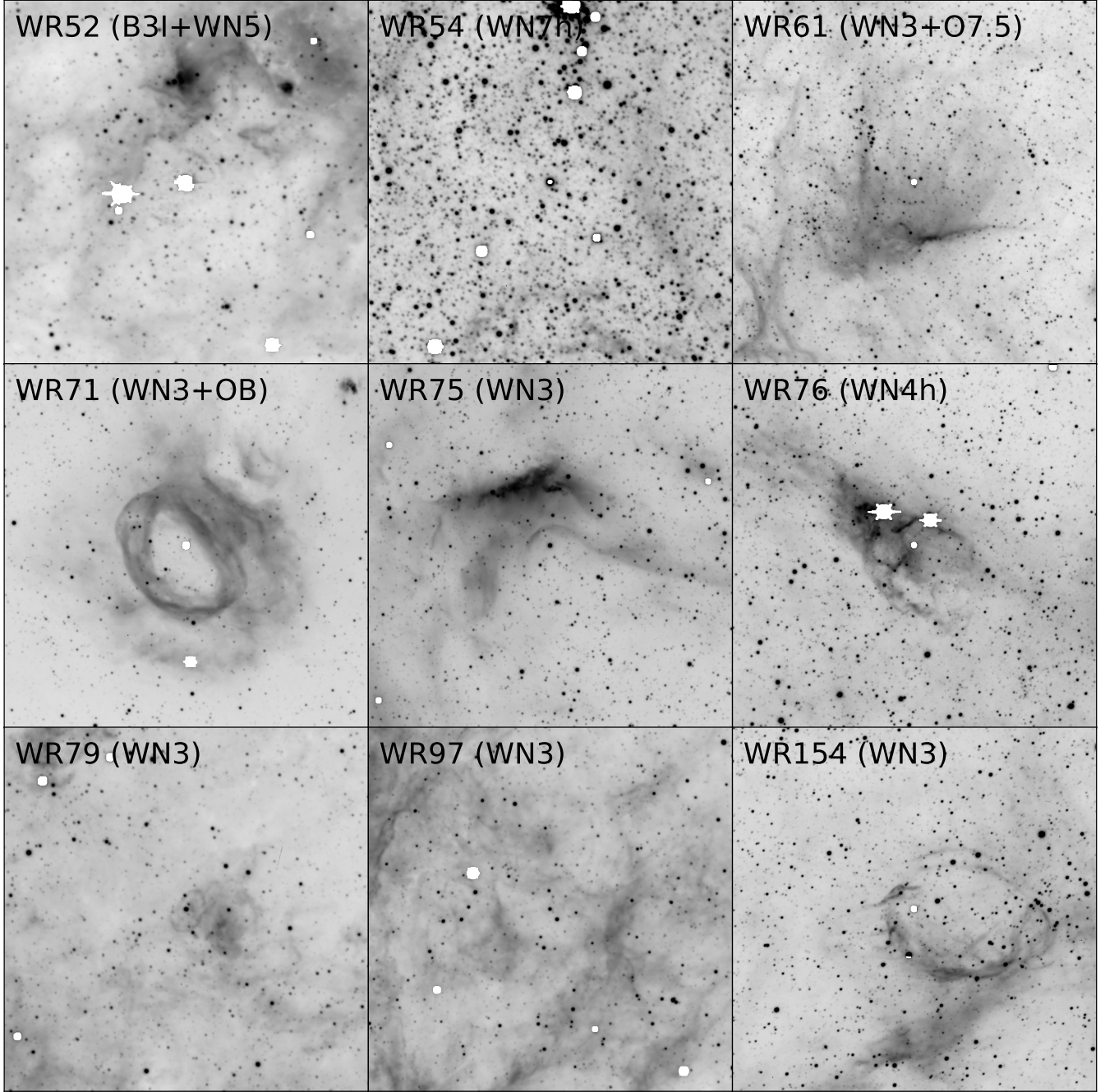
Figure 3. (cont.) 4m MOSAIC Hα images of small bubbles around WR stars in the LMC. The field of view of each panel is 4'$\times$4'. The WR star is at the center of the panel except WR12, which is marked by a red cross.

as a circumstellar bubble expands, its density decreases and its emission measure rapidly drops below the detection limit. (Emission measure $\equiv n^2L$, where n is the electron density and L is the emitting path length). The maximum emission measure of a shell is along the path length tangent to the shell's inner rim. For a uniform shell with mass M, radius R, and fractional shell thickness $\Delta R/R$, the maximum emission measure will be $n^2L = 32^{-1/2}\pi^{-2}R^{-5}(\Delta R/R)^{-3/2}(M/m_H)^2$,

where m_H is the mass of a hydrogen atom. Using observer-friendly units, the emission measure can be expressed in units of cm^{-6} pc as $n^2L \approx 30R^{-5}(\Delta R/R)^{-3/2}M^2$, where n is in units of cm^{-3}, L in parsecs, R in parsecs, and M in $M_\odot$.

It is evident that as the shell expands, the density drops and the maximum emission measure of the shell will decrease rapidly in proportion to R^{-5}. As shown in Figure 5, for a $10\,M_\odot$ shell with $\Delta R/R = 0.05$, the maximum emission mea-
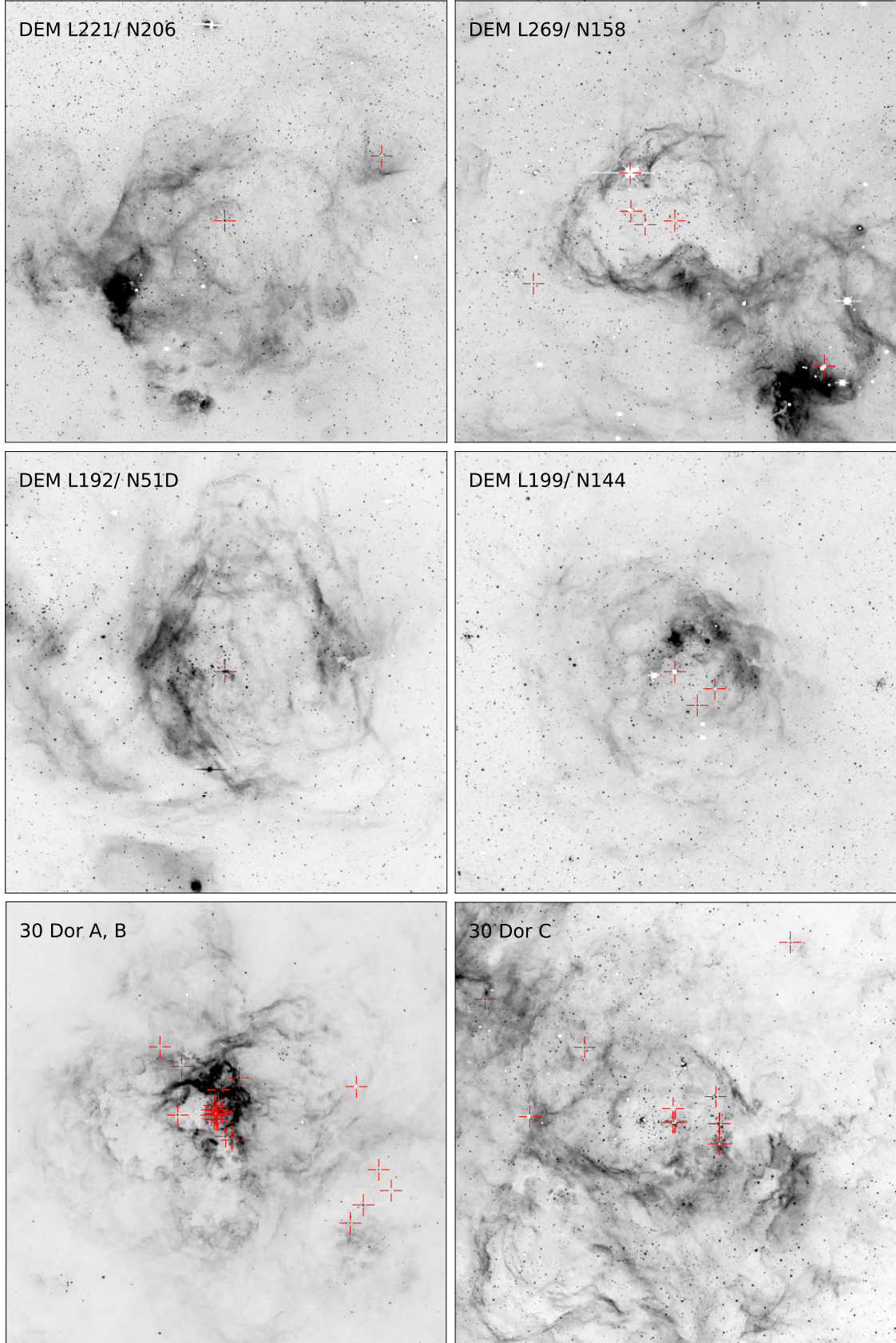
Figure 4. 4m MOSAIC Hα images of example superbubbles around WR stars in the LMC. The field of view of each panel is 15'×15'. The WR stars are marked by red crosses.

sure drops below a detection limit of 10 cm^{-6} pc at a radius of $\sim$8 pc. Therefore, we do not expect to detect a circumstellar bubble around every WR star.

The invisible interstellar bubbles were a puzzle until Nazé et al. (2003) showed that interstellar bubbles blown by MS O stars expand slowly, with expansion velocities of only 15–20 km s^{-1}, producing very weak shocks and compression. Without a large density jump, the interstellar bubble cannot stand out against the background, and the bubble cannot be morphologically identified in direct images. Therefore, interstellar bubbles formed by MS stars are not expected to be seen around WR stars unless the WR star has gone through an RSG phase when the ambient ionized interstellar gas recombines and cools. The isothermal sound velocity of neutral H I gas at 100 K is $\sim$1 km s^{-1}, and an interstellar bubble expanding at 15-20 km s^{-1} would generate strong shocks and compression, causing a large density jump. Such an interstellar bubble will become visible in Hα when the WR phase starts, and the bubble and ambient ISM become photoionized. Whether an interstellar bubble is visible around a WR star depends a lot on the evolutionary path and physical conditions of the ambient ISM.

5.2.2. *Circumstellar versus Interstellar Bubbles*

The most definitive diagnostic of a circumstellar bubble is the N/O abundance ratio (e.g., Esteban et al. 1991). Of the small WR bubbles identified, abundance observations have been made for only three–WR 2, 12, and 19–and only the bubble around WR 19 shows high N/O ratio confirming its circumstellar bubble nature (Garnett & Chu 1994; Stock et al. 2011). The small nebula near WR 47 (BAT99-38) was also observed by Stock et al. (2011); however, this small nebula consists of bright-rimmed Bok globules with embedded star formation (Chu et al. 2005) and not a WR nebula, as described in more detail in the Appendix.

In Section 5.2.1 we have shown that circumstellar bubbles expand and fade below the detection limit when the bubble size is greater than $\sim$20 pc. The smallest WR bubbles are thus more likely to consist of CSM; however, WR 2 and WR 19 have bubbles of similarly small sizes but only the latter shows enhanced N/O ratio. Future spectroscopic observations of the small WR bubbles are needed to determine unambiguously whether they consist of CSM.

5.2.3. *Correlation with Stellar Properties and Environments*

The statistics of small WR bubbles is summarized in Table 6. About 67% of the small bubbles are found around WN2-4 stars, and more strikingly, none of these WN2-4 stars are in OB associations. If all massive stars are born in clusters or OB associations, the absence of OB associations around these WN2-4 stars with small bubbles suggests that the parent OB associations have dissolved after losing the more

massive stars in supernova explosions and that these WN2-4 stars must have lower initial masses, $\sim$25 $M_\odot$. Among WN2-4 stars in superbubbles, only $\sim$50% are in OB associations. This superbubble statistic for WN2-4 stars might be caused by two possible evolutionary paths, with the ones in OB associations more massive than those not in OB associations.

In contrast, two WC4 stars are in small bubbles, and both are in OB associations. This may look like small number statistics, but all 12 WC stars in superbubbles are in OB associations as well. The implication of "WC stars in bubbles and superbubbles are all in OB associations" is intriguing but not clear.

5.3. *Preexisting Environmental Conditions of Supernova Remnants*

Massive as they are, WR stars may explode as core-collapse supernovae near the end of their evolution. We have shown through this survey of bubbles around WR stars that circumstellar bubbles can be observed only at a young age, and as they expand, the density drops and the bubble fades to oblivion. While the interstellar and circumstellar bubbles are not always detected, their shell densities are still above those of the diffuse ISM. Thus, when the central star eventually explodes as a supernova, the supernova ejecta quickly expands in the low-density bubble interior until it hits the circumstellar or interstellar bubble shell. This is called cavity explosion. Supernova remnants formed through cavity explosion include N132D and N63A (Hughes 1987; Hughes et al. 1998), and they are characterized by their large size and high X-ray luminosity.

6. SUMMARY AND CONCLUSION

We have conducted a multiwavelength survey of ISM and CSM around WR stars in the LMC. The latest LMC WR catalog by Neugent et al. (2018) contains 154 entries and should be fairly complete. A number of survey data sets are available for us to probe the ionized and neutral medium around the WR stars: the MCELS images in the Hα, [O III] , and [S II] lines; Blanco 4m Telescope MOSAIC images in the Hα line; *Spitzer Space Telescope* 8 and 24 μm images; and ATCA + Parkes Telescope H I 21 cm line data cube of the LMC.

As a massive star evolves from the MS to WR phase, its fast MS wind turns into a slow RSG or LBV wind and then a fast WR wind. The interactions between these winds and the ambient medium should form a circumstellar bubble inside an interstellar bubble (Garcia-Segura et al. 1996a,b). We expect the interstellar and circumstellar bubbles to be small, <50 pc in size. Our search finds small bubbles around $\sim$12% of WR stars in the LMC, and around $\sim$15% of WR stars in the LMC but outside 30 Dor. Most of these small bubbles
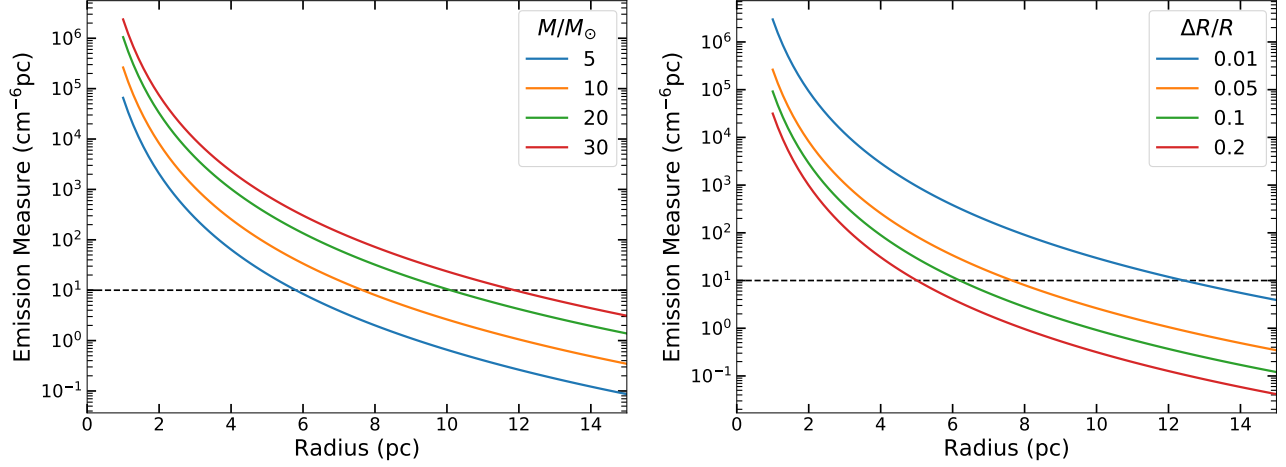
Figure 5. Expected emission measures of circumstellar bubbles for a fixed shell thickness ratio $\Delta R/R = 0.05$ and different bubble masses (left panel), and for $10\,M_\odot$ and different $\Delta R/R$ (right panel). The dashed line marks the emission measure $10\ \mathrm{cm^{-6}}$ pc as the detection limit.

are around WN stars and most of them are not in OB associations. Only the small bubble around WR 19 has a high N/O abundance ratio to confirm its circumstellar bubble nature. The scarcity of small bubbles can be caused by several factors. As a bubble expands, its surface brightness drops in proportion to (radius)$^{-5}$ and fades below the detection limit within a short time. Furthermore, it has been observed that interstellar bubbles expand at 15–20 km s^{-1}, which cannot produce strong compression for the bubble shell to stand out against the background; thus, interstellar bubbles can be diagnosed kinematically but not morphologically (Nazé et al. 2003).

WR stars and nearby massive stars can jointly blow a superbubble with their fast stellar winds and supernova explosions. In 30 Dor, 63% of its 46 WR stars are in superbubbles, and 28 of the 29 WR stars in superbubbles are also in OB associations. Outside 30 Dor, only 33% of the 110 WR stars are in superbubbles; about two-thirds of these WR stars in superbubbles are also in OB associations. The contrasting statistics is caused by the prominent starburst in 30 Dor that produced the massive OB association LH 90 in 30 Dor C and more impressively the super star cluster R136 (LH 100) in the central superbubble of 30 Dor A. While both inside and outside 30 Dor WN stars contribute to ∼80% of the WR population, the number ratio of WN2-4 to WN5-6 stars is 1:3 in 30 Dor and 8:1 outside 30 Dor. The dominant WN4-5 stars in 30 Dor are probably massive H-burning stars.

We have also classified the H II environments of WR stars into three categories: class 1 for bright amorphous H II regions; class 2 for shell H II regions, such as superbubbles; and class 3 for low-density diffuse medium. These three classes correspond to a progression in the dynamical dispersal of ISM around massive stars. Inside 30 Dor, the distribution of WR stars in classes 1-3 is 15%, 72%, and 13%, respectively. The stars in class 3 H II environments are in the

outskirts of 30 Dor. Outside 30 Dor, the distribution of WR stars in classes 1–3 is 5%, 36%, and 58%, respectively. The contrast between 30 Dor and elsewhere reflects the age and mass differences in the WR star population. For example, among the 65 WN2-4 stars outside 30 Dor, about 68% are not in OB associations and 63% are in class 3 H II environments. The WN2-4 stars not in OB associations and in class 3 H II environments are most likely He-burning WR stars from progenitors with initial masses below ∼30 $M_\odot$.

Finally, spectroscopic analyses of abundances are needed to determine whether the small WR bubbles contain ISM or CSM. It is important to determine the physical properties and nature of small WR bubbles, as they will define how the future supernova remnants develop.

Table 1. LMC WR Stars and Their Stellar and Interstellar Environments

WR #	α(J2000)	δ(J2000)	BAT99 Num.	Brey Num.	Spectral Type	OB assc. [a] LH Num.	Nebula Henize N	Nebula DEM L	H II Morphology	Bubble (arcmin)	Superbubble (arcmin)	H II SGS LMC-	H I Shell [b]
(1)	(2)	(3)	(4)	(5)	(6)	(7)	(8)	(9)	(10)	(11)	(12)	(13)	(14)
1	04 45 32.25	-70 15 10.9	1	1	WN3	...	...	...	3c	...	...	...	...
2	04 49 36.25	-69 20 54.8	2	2	WN2	...	79	6	2a	0.4 × 0.3	3.2 × 2.2	...	...
3	04 52 57.39	-66 41 13.5	3	3	WN3	...	...	...	3c	...	...	...	...
4	04 53 03.76	-69 23 51.8	...	...	WN3+O6V	((2))	...	10	2a	0.6 × 0.6	4.3 × 4	7	GS 9
5	04 53 30.08	-69 17 49.4	4	3a	WNL/Of?	((5))	...	...	3b	...	18 × 12	7	GS 9
6	04 54 28.10	-69 12 50.9	5	4	WN2	5	83	22	3a	...	...	7	GS 15
7	04 55 07.60	-69 12 31.7	5a	...	WN3	((5))	...	22	3a	...	...	7	GS 15
8	04 55 31.35	-67 30 02.7	7	...	WN3pec	...	...	...	3b	...	11 × 7.6	...	...
9	04 56 02.88	-69 27 21.5	8	8	WC4	8	94	36	2b	...	7.6 × 6.6	7	GS 18
10	04 56 11.0	-66 17 33.0	9	7	WC4	...	11	34	2a	...	(4 × 2)	...	GS 16
11	04 56 34.63	-66 28 26.4	10	9	WC4+OB	9	11	34	2a	...	12 × 8	...	GS 16
12	04 57 24.10	-68 23 57.3	11	10	WC4	12	91	39	1/2a	3 × 2	...	6	SGS 2
13	04 56 48.79	-69 36 40.7	...	...	WN4/O4	...	...	...	3c	...	...	7	GS 18
14	04 57 27.44	-67 39 02.9	12	...	O2If*/WN5	...	...	40	3a	2.2 × 1.4	...	...	...
15	04 57 41.04	-66 32 42.6	13	...	WN10	...	11	34	3a	...	...	...	...
16	04 58 56.36	-68 48 04.7	14	11	WN4+OB	...	...	...	3c	...	...	6	SGS 2
17	04 59 51.55	-67 56 55.4	15	12	WN3	...	16A	45	2a	2 × 2	10.2 × 8.4	...	...
18	05 02 59.24	-69 14 02.3	15a	...	WN3+abs	...	...	...	3b	...	20 × 20	...	...
19	05 03 08.91	-66 40 57.5	16	13	WN7h	...	...	5	3a	0.7 × 0.3	...	...	...
20	05 04 12.33	-70 03 55.4	17	14	WN4	...	...	68	3a/3b	...	7.7 × 4.3	8	...
21	05 04 32.64	-68 00 59.4	...	...	WN3/O3	...	23	66	2a	3 × 2.8	...	...	SGS 5
22	05 05 08.43	-70 22 45.1	18	15	WN3h	...	...	80	3c	...	...	8	...
23	05 07 13.33	-70 33 33.9	...	...	WN3/O3	((26))	...	80	3a	...	...	8	...
24	05 09 40.42	-68 53 24.8	19	16	WN3+OB	31	105A	86	2a	...	4.4 × 3	...	SGS 5
25	05 09 53.77	-68 52 52.5	20	16a	WC4	31	105A	86	1/2a	2.8 × 1.4	...	...	SGS 5
26	05 13 43.77	-67 22 29.4	21	17	WN4+OB	37	30	105	(2b)	...	(10.2 × 7.4)	...	GS 44
27	05 13 54.27	-69 31 46.7	22	18	WN9	39	...	110	2b	...	7 × 4.6	...	GS 45

Table 1 *continued*

Table 1 (*continued*)

WR #	α(J2000)	δ(J2000)	BAT99 Num.	Brey Num.	Spectral Type	OB assc. LH Num.[a]	Nebula Henize N	Nebula DEM L	H II Morphology	Bubble (arcmin)	Superbubble (arcmin)	H II SGS LMC-	H I Shell[b]
(1)	(2)	(3)	(4)	(5)	(6)	(7)	(8)	(9)	(10)	(11)	(12)	(13)	(14)
28	05 13 56.01	−67 24 36.6	23	...	WN3	(37)/(38)	30	105	3a	...	...	...	GS 44
29	05 14 12.69	−69 19 26.2	24	19	WN3	(35)	113	108	2a	2.8 × 2.6	...	...	GS 46
30	05 14 17.57	−67 20 35.1	...	...	O3.5If*/WN5	(36)	30	105	2b	...	10.2 × 7.4	...	GS 44
31	05 14 57.27	−71 36 18.3	25	19a	WN4ha	...	...	119	3a	...	...	...	GS 47
32	05 16 38.84	−69 16 40.9	26	20	WN4	...	119	...	3a/3c	...	...	...	GS 51
33	05 18 10.33	−69 13 02.5	...	...	WO4	41	119	132a	3a	...	...	...	GS 54
34	05 18 10.88	−69 13 11.4	...	...	WO4	41	119	132a	3a	...	...	...	GS 54
35	05 18 19.21	−69 11 40.7	27	21	B1+WN4	41	119	132b	3a/3b	...	...	...	GS 54
36	05 19 16.34	−69 39 20.0	28	22	WC6+O5-6	42	120	134	3a	...	...	...	...
37	05 20 44.73	−65 28 20.5	29	23	WN3+OB	43	...	137	2b	...	13.8 × 12.8	...	SGS 6
38	05 21 22.82	−65 52 48.8	...	...	WN3/O3	45	...	154	3a/3b	...	...	5	SGS 7
39	05 21 57.70	−65 49 00.3	30	24	WN6h	45	...	154	3b	...	...	5	SGS 7
40	05 22 04.41	−67 59 06.8	31	25	WN3	47	44C	152	1	...	...	...	...
41	05 22 22.53	−71 35 58.1	32	26	WN6h	...	198	165	2b	...	8.1 × 5.5	...	GS 61
42	05 22 59.78	−68 01 46.6	33	...	Ofpe/WN9	49	44	160	1	...	...	...	...
43	05 23 10.06	−71 20 50.9	34	28	WC4+abs	50	200	164	2b	...	15.4 × 12.7	9	GS 61
44	05 23 18.01	−65 56 57.0	35	27	WN3	...	...	154	3c	...	...	5	SGS 7
45	05 24 24.19	−68 31 35.6	36	29	WN3/WCE+OB	...	138	174	1	...	...	3	...
46	05 24 54.34	−66 14 11.1	37	30	WN3	((52))	...	175	2b	...	7.6 × 3.8	5	SGS 7
47	05 26 03.96	−67 29 57.1	38	31	WC4+abs	54	51D	192	2b	...	12 × 9.5	4	SGS 11
48	05 24 56.87	−66 26 44.4	...	...	WN3/O3	...	48E	175a	2b	(3.8 × 2.9)	...	4, 5	SGS 7, 11
49	05 26 30.26	−68 50 27.5	39	32	WC4+O6III/V	58	144	199	2a	...	10 × 10	3	SGS 12
50	05 26 36.86	−68 51 01.3	40	33	WN4	58	144	199	2a	...	10 × 10	3	SGS 12
51	05 26 42.58	−69 06 57.4	41	35	WN4	...	135	198	3a	...	...	3	SGS 12
52	05 26 45.32	−68 49 52.8	42	34	B3I+WN5	58	144	199	2a	0.8 × 0.8	10 × 10	3	SGS 12
53	05 27 37.68	−70 36 05.4	43	37	WN3+OB	62	204	208	2a/2b	...	14.4 × 13.5	9	...
54	05 27 42.69	−69 10 00.4	44	36	WN7h	...	135	210	3b	3.0 × 2.4	...	3	SGS 12
55	05 27 52.66	−68 59 08.5	45	...	WN10→LBV	61	135	210	3a	...	...	3	SGS 12
56	05 28 17.90	−69 02 35.9	46	38	WN4	((61))	135	210	3a	...	...	3	SGS 12

Table 1 *continued*

Table 1 (*continued*)

WR #	α(J2000)	δ(J2000)	BAT99 Num.	Brey Num.	Spectral Type	OB assc.[a] LH Num.	Nebula Henize N	Nebula DEM L	H II Morphology	Bubble (arcmin)	Superbubble (arcmin)	H II SGS LMC-	H I Shell[b]
(1)	(2)	(3)	(4)	(5)	(6)	(7)	(8)	(9)	(10)	(11)	(12)	(13)	(14)
57	05 28 27.12	-69 06 36.2	...	...	WN3/O3	...	135	210	3a	...	...	3	SGS 12
58	05 29 12.37	-68 45 36.1	47	39	WN3	64	135	...	3c	...	...	3	SGS 12
59	05 29 18.19	-69 19 43.2	...	...	WN3/O3	...	135	...	3c	...	...	3	SGS 12
60	05 29 31.64	-68 54 28.8	48	40	WN3	...	135	...	3c	...	...	3	SGS 12
61	05 29 33.21	-70 59 34.9	49	40a	WN3+O7.5	((66))	206	221	2a	1.4 × 1.4	14 × 11	9	GS 70
62	05 29 53.64	-69 01 04.8	50	41	WN5h	...	135	...	3c	...	...	3	SGS 12
63	05 30 02.46	-68 45 18.4	51	42	WN 3	((64))	135	218	3c	...	...	3	SGS 12
64	05 30 12.16	-67 26 08.3	52	43	WC4	...	...	...	3c	...	...	4	SGS 11
65	05 30 38.70	-71 01 47.8	53	44	WC4+abs	69	206	221	2a	...	14 × 11	9	GS 70
66	05 31 18.05	-69 08 45.5	54	...	WN9	...	135	232	3a	...	...	3	SGS 12
67	05 31 25.52	-69 05 38.6	55	...	WN11	...	135	232	3a	...	...	3	SGS 12
68	05 31 32.87	-67 40 46.6	56	46	WN3	((76))	57	229	2a	...	11.5 × 6.5	4	...
69	05 31 34.36	-67 16 29.3	57	45	WN3	((70))	...	...	3a	...	...	4	SGS 11
70	05 32 07.49	-68 26 31.6	58	47	WN7h	...	148	227	3a	...	...	3	SGS 12
71	05 33 10.57	-67 42 43.1	59	48	WN3+OB	((76))	57C	231	2b	1.5 × 1.2	...	...	...
72	05 33 10.87	-69 29 01.0	60	49	WN3+OB	...	135	224	3a	...	...	...	...
73	05 34 19.24	-69 45 10.3	61	50	WC4	81	154	246	2a	...	21 × 15	...	GS 73
74	05 34 36.08	-69 45 36.5	...	...	B0I+WN	81	154	246	2a	...	21 × 15	...	GS 73
75	05 34 37.47	-66 14 38.0	62	51	WN3	...	62A	239	3a	0.7 × 0.2	...	4	SGS 11
76	05 34 52.03	-67 21 29.0	63	52	WN4h	...	...	240	3a	1.5 × 1.1	...	4	SGS 11
77	05 34 59.38	-69 44 06.3	64	53	WN3+O	81	154	246	2a	...	21 × 15	...	GS 73
78	05 35 00.90	-69 21 20.2	...	...	WN3/O3	...	157	263	3a	...	...	...	...
79	05 35 15.18	-69 05 43.1	65	55	WN3	((89))	157	263	3a	0.5 × 0.3	...	...	...
80	05 35 28.52	-69 40 08.9	...	...	WN3+O8-9III	87	154	246	2a	...	21 × 15	...	GS 73
81	05 35 29.80	-67 06 49.4	66	54	WN3(h)	...	...	...	3a	...	...	4	SGS 11
82	05 35 41.96	-69 11 52.9	69	...	WC4	90	157C	263	2b	...	7.5 × 5.2	...	GS 75
83	05 35 42.19	-69 12 34.5	67	56	WN5h	90	157C	263	2b	...	7.5 × 5.2	...	GS 75
84	05 35 42.20	-69 11 53.6	68	58	O3.5If*/WN7	90	157C	263	2b	...	7.5 × 5.2	...	GS 75
85	05 35 43.49	-69 10 58.0	70	62	WC4	90	157C	263	2b	...	7.5 × 5.2	...	GS 75

Table 1 *continued*

Table 1 (*continued*)

WR #	α(J2000)	δ(J2000)	BAT99 Num.	Brey Num.	Spectral Type	OB assc.[a] LH Num.	Nebula Henize N	Nebula DEM L	H II Morphology	Bubble (arcmin)	Superbubble (arcmin)	H II SGS LMC-	H I Shell[b]
(1)	(2)	(3)	(4)	(5)	(6)	(7)	(8)	(9)	(10)	(11)	(12)	(13)	(14)
86	05 35 44.28	-68 59 36.8	71	60	WN3+abs	89	135	...	3a	...	...	3	...
87	05 35 45.03	-68 58 44.4	72	61	WN4+abs	89	135	...	3a	...	...	3	...
88	05 35 50.65	-68 53 39.2	73	63	WN5	85	135	...	3a	...	...	3	...
89	05 35 52.43	-68 55 08.7	74	63a	WN3+abs	89	135	...	3a	...	...	3	...
90	05 35 54.03	-67 02 48.9	75	59	WN4	...	...	...	3c	...	...	4	SGS 11
91	05 35 54.37	-68 59 07.9	76	...	WN9	89	135	...	3a	...	...	3	...
92	05 35 58.87	-69 11 47.8	77	65	WN7	90	157C	263	2b	...	7.5 × 5.2	...	GS75
93	05 35 59.16	-69 11 50.7	78	65b	WN4	90	157C	263	2b	...	7.5 × 5.2	...	GS75
94	05 35 59.82	-69 11 22.3	79	57	WN7	90	157C	263	2b	...	7.5 × 5.2	...	GS75
95	05 35 59.89	-69 11 50.6	80	...	WN5	90	157C	263	2b	...	7.5 × 5.2	...	GS75
96	05 36 12.13	-67 34 57.8	81	65a	WN5h	88	59B	241	2a	...	...	...	...
97	05 36 33.58	-69 09 17.3	82	66	WN3	(90)	157	263	2b	1.5 × 0.7	(6.6 × 2.7)	...	...
98	05 36 43.71	-69 29 47.5	83	...	Ofpe/WN9→LBV	94	135	248	3c	...	...	...	...
99	05 36 51.38	-69 25 56.7	84	68	WC4(+OB)	96	135	261	3b	...	6.9 × 5.2	...	...
100	05 36 54.66	-69 11 38.3	85	67	WC4(+OB)	((90))	157	263	3a	...	...	...	...
101	05 37 11.48	-69 07 38.2	86	69	WN3	(100)	157A	263	3a	...	...	...	...
102	05 37 29.24	-69 20 47.5	87	70	WC4	97	135	261	3a	...	...	...	...
103	05 37 35.72	-69 08 40.3	88	70a	WN3/WCE	(99)	157A	263	3a	...	...	...	...
104	05 37 40.50	-69 07 57.7	89	71	WN6	(99)	157A	263	3a	...	...	...	...
105	05 37 44.64	-69 14 25.7	90	74	WC4	(99)	157	263	3a	...	...	...	...
106	05 37 46.35	-69 09 09.6	91	73	WN6h	99	157B	263	3a	...	...	...	...
107	05 37 47.62	-69 21 13.6	...	...	WN3+O7V	97	135	261	3b	...	(4.3 × 1.6)	...	...
108	05 37 49.04	-69 05 08.3	92	72	B1I+WN3	((99,100))	157A	263	2a	...	8 × 7	...	...
109	05 37 51.34	-69 09 46.7	93	...	O3If*	99	157B	263	1	...	...	...	...
110	05 38 24.21	-69 29 13.4	...	...	WN11	101	158	269	3a	...	...	...	...
111	05 38 27.71	-69 29 58.5	94	85	WN3/4pec	101	158	269	3a	...	...	...	...
112	05 38 33.62	-69 04 50.5	95	80	WN7	(100)	157A	263	1	...	...	...	GS78
113	05 38 36.42	-69 06 57.4	96	81	WN7	(100)	157A	263	1	...	...	...	GS78
114	05 38 38.84	-69 06 49.5	97	...	O3.5If*/WN7	(100)	157A	263	1	...	...	...	GS78

Table 1 *continued*

Table 1 (*continued*)

WR #	α(J2000)	δ(J2000)	BAT99 Num.	Brey Num.	Spectral Type	OB assc.[a] LH Num.	Nebula Henize N	Nebula DEM L	H II Morphology	Bubble (arcmin)	Superbubble (arcmin)	H II SGS LMC-	H I Shell[b]
(1)	(2)	(3)	(4)	(5)	(6)	(7)	(8)	(9)	(10)	(11)	(12)	(13)	(14)
115	05 38 39.15	-69 06 21.2	98	79	WN6	100	157A	263	2a	...	2.5 × 1.4	...	GS 78
116	05 38 40.23	-69 05 59.8	99	...	O2.5If*/WN6	100	157A	263	2a	...	2.5 × 1.4	...	GS 78
117	05 38 40.55	-69 05 57.1	100	...	WN6h	100	157A	263	2a	...	2.5 × 1.4	...	GS 78
118	05 38 41.60	-69 05 14.0	101	...	WC4	100	157A	263	2b	(1.1 × 0.9)	...	...	GS 78
119	05 38 41.60	-69 05 14.0	102	...	WN6	100	157A	263	2b	(1.1 × 0.9)	...	...	GS 78
120	05 38 41.62	-69 05 15.1	103	...	WN5(h)+O	100	157A	263	2b	(1.1 × 0.9)	...	...	GS 78
121	05 38 41.88	-69 06 14.4	104	...	O2If*/WN5	100	157A	263	2a	...	2.5 × 1.4	...	GS 78
122	05 38 42.12	-69 05 55.2	105	...	O2If*	100	157A	263	2a	...	2.5 × 1.4	...	GS 78
123	05 38 42.33	-69 06 03.3	106	...	WN4.5h	100	157A	263	2a	...	2.5 × 1.4	...	GS 78
124	05 38 42.39	-69 06 02.9	108	...	WN5h	100	157A	263	2a	...	2.5 × 1.4	...	GS 78
125	05 38 42.41	-69 06 15.0	...	...	O2If*/WN5	100	157A	263	2a	...	2.5 × 1.4	...	GS 78
126	05 38 42.41	-69 06 02.9	109	...	WN5h	100	157A	263	2a	...	2.5 × 1.4	...	GS 78
127	05 38 42.43	-69 06 02.7	110	...	O2If*/O3If*/WN6	100	157A	263	2a	...	2.5 × 1.4	...	GS 78
128	05 38 42.91	-69 06 04.8	112	...	WN4.5h	100	157A	263	2a	...	2.5 × 1.4	...	GS 78
129	05 38 43.10	-69 05 46.8	113	...	O2If*/WN5	100	157A	263	2a	...	2.5 × 1.4	...	GS 78
130	05 38 43.21	-69 06 14.4	114	...	O2If*/WN5	100	157A	263	2a	...	2.5 × 1.4	...	GS 78
131	05 38 44.06	-69 05 55.6	115	...	WC5	100	157A	263	2a	...	2.5 × 1.4	...	GS 78
132	05 38 44.26	-69 06 05.9	116	...	WN4.5h	100	157A	263	2a	...	2.5 × 1.4	...	GS 78
133	05 38 47.52	-69 00 25.3	117	88	WN4.5	100	157A	263	2a	...	8 × 4	...	...
134	05 38 53.38	-69 02 00.9	118	...	WN5/6+WN6/7	100	157A	263	2a	...	8 × 4	...	...
135	05 38 55.53	-69 04 26.7	...	...	WN5h	(100)	157A	263	1	...	...	...	GS 78
136	05 38 57.07	-69 06 05.7	119	90	WN6+O3.5If*/WN7	100	157A	263	2a	...	2.5 × 1.4	...	GS 78
137	05 38 58.09	-69 29 19.5	120	91	WN9	101	158	269	1	...	...	...	...
138	05 39 03.78	-69 03 46.5	121	...	WC4	(100)	157A	263	1	...	...	...	...
139	05 39 11.33	-69 02 01.6	122	92	WN5h	((100))	157A	263	1	...	...	...	...
140	05 39 34.29	-68 44 09.2	123	93	WO3	...	...	268	3a	...	...	...	...
141	05 39 36.18	-69 39 11.2	124	93a	WN3	103	160	284	1	...	...	2	SGS 19
142	05 39 56.11	-69 24 24.3	125	94	WC4+abs	104	158	269	2a	...	7.5 × 6.3	2	SGS 19
143	05 40 03.57	-69 37 53.1	...	...	WN3/O3	103	160	284	2a	...	12 × 8	2	SGS 19

Table 1 *continued*

Table 1 (*continued*)

WR #	α(J2000)	δ(J2000)	BAT99 Num.	Brey Num.	Spectral Type	OB assc.[a] LH Num.	Nebula Henize N	Nebula DEM L	H II Morphology	Bubble (arcmin)	Superbubble (arcmin)	H II SGS LMC-	H I Shell[b]
(1)	(2)	(3)	(4)	(5)	(6)	(7)	(8)	(9)	(10)	(11)	(12)	(13)	(14)
144	05 40 07.55	-69 24 31.9	126	95	WN3+O7	104	158	269	2a	...	7.5 × 6.3	2	SGS 19
145	05 40 13.06	-69 24 04.2	127	...	WC4+O	104	158	269	2a	...	7.5 × 6.3	2	SGS 19
146	05 40 13.33	-69 22 46.5	...	...	B[e]+WN?	104	158	269	2a	...	7.5 × 6.3	2	SGS 19
147	05 40 50.80	-69 26 31.8	128	96	WN3	(104)	158	269	3a	...	...	2	SGS 19
148	05 41 17.50	-69 06 56.2	...	...	WN3/O3	...	135	310	3a	(2.8 × 1.8)	(6.3 × 4.5)	2	SGS 19
149	05 41 48.57	-70 35 30.8	129	97	WN3+O5V	...	...	294	3a	...	...	...	...
150	05 44 31.03	-69 20 15.5	130	...	WN11	...	135	310	3a	...	...	2	SGS 19
151	05 44 53.72	-67 10 36.2	131	98	WN4	116	74	309	2a	...	17 × 15	...	GS 94
152	05 45 24.16	-67 05 56.8	132	99	WN4	((116))	...	309	3c	...	...	...	...
153	05 45 51.93	-67 14 25.9	133	...	WN11	((116))	...	308	2a	...	17 × 15	...	GS 94
154	05 46 46.35	-67 09 58.3	134	100	WN3	...	74	315	2a	1.8 × 1.3	7.5 × 5.2	...	GS 94

[a] Single parentheses around OB association indicate that the star is within 50 pc of the center of the OB association, double parentheses indicate that the star is within 100 pc, and no parentheses indicate that the star is within the association. Ellipses indicate no association.

[b] GS: giant shell, SGS: supergiant shell.

Table 2. WR Stars with Small Bubbles

WR #	Spectral Type	Dimensions		Nebula	OB
		(arcmin)	(pc)	DEM L	LH
(1)	(2)	(3)	(4)	(5)	(6)
2	WN2	0.4×0.3	6×4.5	6	...
4	WN3+O6V	0.6×0.6	9×9	10	((2))
12	WC4	3×2	45×30	39	12
14	O2If*/WN5	2.2×1.4	33×21	40	...
17	WN3	2×2	30×30	45	...
19	WN7h	0.7×0.3	10.5×4.5	5	...
21	WN3/O3	3×2.8	45×42	66	...
25	WC4	2.8×1.4	42×21	86	31
29	WN3	2.8×2.6	42×39	108	(35)
52	B3I+WN5	0.8×0.8	12×12	199	58
54	WN7h	3.0×2.4	45×36	210	...
61	WN3+O7.5	1.4×1.4	21×21	221	((66))
71	WN3+OB	1.5×1.2	22.5×18	231	((76))
75	WN3	0.7×0.2	10.5×3	239	...
76	WN4h	1.5×1.1	22.5×16.5	240	...
79	WN3	0.5×0.3	7.5×4.5	263	((89))
154	WN3	1.8×1.3	27×19.5	315	...
97 †	WN3	1.5×0.7	22.5×10.5	263	(90)

NOTE—† In 30 Dor.

Table 3. WR Stars in Superbubbles (Excluding 30 Dor)

| WR # | Spectral Type | Dimensions | | Nebula | OB |
| | | (arcmin) | (pc) | DEM L | LH |
(1)	(2)	(3)	(4)	(5)	(6)
2	WN2	3.2 × 2.2	48 × 33	6	...
4	WN3+O6V	4.3 × 4	64.5 × 60	10	((2))
5	WNL/Of?	18 × 12	270 × 180	...	((5))
8	WN3pec	11 × 7.6	165 × 114	...	...
9	WN3	7.6 × 6.6	114 × 99	36	8
11	WC4+OB	12 × 8	180 × 120	34	9
17	WN3	10.2 × 8.4	153 × 126	45	...
18	WN3+abs	20 × 20	300 × 300	...	...
20	WN4	7.7 × 4.3	115.5 × 64.5	68	...
24	WN3+OB	4.4 × 3	66 × 45	86	31
27	WN9	7 × 4.6	105 × 69	110	39
30	O3.5If*/WN5	10.2 × 7.4	153 × 111	105	(36)
37	WN3+OB	13.8 × 12.8	207 × 192	137	43
41	WN6h	7.7 × 5.5	115.5 × 82.5	165	...
43	WC4+abs	15.4 × 12.7	231 × 190.5	164	50
46	WN3	7.6 × 3.8	114 × 57	175	((52))
47	WC4+abs	12 × 9.5	180 × 142.5	192	54
49	WC4+O6III/V	10 × 10	150 × 150	199	58
50	WN4	10 × 10	150 × 150	199	58
52	B3I+WN5	10 × 10	150 × 150	199	58
53	WN3+OB	14.4 × 13.5	216 × 202.5	208	62
61	WN3+O7.5	14 × 11	210 × 165	221	((66))
65	WC4+abs	14 × 11	210 × 165	221	69
68	WN3	11.5 × 6.5	172.5 × 97.5	229	((76))
73	WC4	21 × 15	315 × 225	246	81
74	B0I+WN	21 × 15	315 × 225	246	81
77	WN3+O	21 × 15	315 × 225	246	81
80	WN3+O8-9III	21 × 15	315 × 225	246	87
99	WC4(+OB)	6.9 × 5.2	103.5 × 78	261	96
142	WC4+abs	7.5 × 6.3	112.5 × 94.5	269	104
143	WN3/O3	12 × 8	180 × 120	284	103
144	WN3+O7	7.5 × 6.3	112.5 × 94.5	269	104
145	WC4+O	7.5 × 6.3	112.5 × 94.5	269	104
151	WN4	17 × 15	255 × 225	309	116
153	WN11	17 × 15	255 × 225	308	((116))
154	WN3	7.7 × 5.5	115.5 × 82.5	315	...

Table 4. WR Stars in Superbubbles in 30 Dor

WR #	Spectral Type	Dimensions		Nebula	OB
		(arcmin)	(pc)	Name	
(1)	(2)	(3)	(4)	(5)	(6)
82	WC4	7.5 × 5.2	112.5 × 78	N157C	90
83	WN5h	7.5 × 5.2	112.5 × 78	N157C	90
84	O3.5If*/WN7	7.5 × 5.2	112.5 × 78	N157C	90
85	WC4	7.5 × 5.2	112.5 × 78	N157C	90
92	WN7	7.5 × 5.2	112.5 × 78	N157C	90
93	WN4	7.5 × 5.2	112.5 × 78	N157C	90
94	WN7	7.5 × 5.2	112.5 × 78	N157C	90
95	WN5	7.5 × 5.2	112.5 × 78	N157C	90
108	B1I+WN3	8 × 7	120 × 105	Shell 3	...
115	WN6	2.5 × 1.4	37.5 × 21	Central Shell	100
116	O2.5If*/WN6	2.5 × 1.4	37.5 × 21	Central Shell	100
117	WN6h	2.5 × 1.4	37.5 × 21	Central Shell	100
121	O2If*/WN5	2.5 × 1.4	37.5 × 21	Central Shell	100
122	O2If*	2.5 × 1.4	37.5 × 21	Central Shell	100
123	WN4.5h	2.5 × 1.4	37.5 × 21	Central Shell	100
124	WN5h	2.5 × 1.4	37.5 × 21	Central Shell	100
125	O2If*/WN5	2.5 × 1.4	37.5 × 21	Central Shell	100
126	WN5h	2.5 × 1.4	37.5 × 21	Central Shell	100
127	O2If*/O3If*/WN6	2.5 × 1.4	37.5 × 21	Central Shell	100
128	WN4.5h	2.5 × 1.4	37.5 × 21	Central Shell	100
129	O2If*/WN5	2.5 × 1.4	37.5 × 21	Central Shell	100
130	O2If*/WN5	2.5 × 1.4	37.5 × 21	Central Shell	100
131	WC5	2.5 × 1.4	37.5 × 21	Central Shell	100
132	WN4.5h	2.5 × 1.4	37.5 × 21	Central Shell	100
133	WN4.5	8 × 4	120 × 60	Shell 5	100
134	WN5/6+WN6/7	8 × 4	120 × 60	Shell 5	100
136	WN6+O3.5If*/WN7	2.5 × 1.4	37.5 × 21	Central Shell	100

Table 5. LMC WR Stars in LH OB Associations

Spec. Type	The LMC		The LMC − 30 Dor		30 Dor	
	# WR	# WR in OB	# WR	# WR in OB	# WR	# WR in OB
(1)	(2)	(3)	(4)	(5)	(6)	(7)
WN2-4	72	24 (33%)	65	21 (32%)	7	3 (43%)
WN5-6	31	23 (74%)	8	4 (50%)	23	19 (83%)
WN7-L	23	11 (48%)	16	7 (44%)	7	4 (57%)
WC4	21	16 (76%)	15	13 (87%)	6	3 (50%)
WC5-6	2	2 (...)	1	1 (...)	1	1 (...)
WO3-4	3	2 (...)	3	2 (...)	0	0 (...)
Other	4	4 (...)	2	2 (...)	2	2 (...)
Total	156	82 (53%)	110	50 (45%)	46	32 (70%)

Table 6. Spectral Types of WR Stars in Bubbles and Superbubbles

	The LMC				The LMC - 30 Dor				30 Dor	
Spectral Type	# of WR in Bubbles	In OB Assc.	# of WR in Superbubbles	In OB Assc.	# of WR in Bubble	In OB Assc.	# of WR in Superbubbles	In OB Assc.	# of WR in Superbubbles	In OB Assc.
(1)	(2)	(3)	(4)	(5)	(6)	(7)	(8)	(9)	(10)	(11)
WN2-4	12 (17%)	0	24 (33%)	13	11 (17%)	0	20 (31%)	10	4 (57%)	3
WN5-6	2 (6%)	1	20 (65%)	18	2 (25%)	1	3 (38%)	1	17 (74%)	17
WN7-L	2 (9%)	0	7 (30%)	5	2 (13%)	0	3 (19%)	1	4 (...)	4
WC4	2 (10%)	2	11 (52%)	11	2 (13%)	2	9 (60%)	9	2 (...)	2
WC5-6	0 (...)	0	1 (...)	1	0 (...)	0	0 (...)	0	1 (...)	1
WO3-4	0 (...)	0	0 (...)	0	0 (...)	0	0 (...)	0	0 (...)	0
Other	0 (...)	1	2 (...)	2	0 (...)	0	1 (...)	1	1 (...)	1
Total	18 (12%)	4	65 (42%)	50	17 (15%)	3	36 (33%)	22	29 (63%)	28

Table 7. H II Region Morphology Classes of Different Types of WR Stars

	The LMC			LMC–30 Dor			30 Dor		
Spectral Type	H II Classes			H II Classes			H II Classes		
	1	2	3	1	2	3	1	2	3
WN2-4	3	26	43	3	21	41	0	5	2
WN5-6	2	23	6	0	4	4	2	19	2
WN7-L	5	6	12	2	2	12	3	4	0
WC4	2	14	5	1	11	3	1	3	2
WC5-6	0	1	1	0	0	1	0	1	0
WO3-4	0	0	3	0	0	3	0	0	0
Other	1	3	0	0	2	0	1	1	0
Total	13	73	70	6	40	64	7	33	6

APPENDIX

In this appendix, the nomenclature for OB associations, H I and H II features are abbreviated as the following:

LHn – OB association from Lucke & Hodge (1970),
Nn – LHα 120-Nn H II region from Henize (1956),
DEM Ln – LMC H II region from Davies et al. (1976),
H II SGS LMC-n – ionized SGS identified from Hα images by Meaburn (1980),
H I GS n – H I giant shell from Kim et al. (1999), and
H I SGS n – H I SGS from Kim et al. (1999).

WR1 is in a field without any nebulosity in the vicinity or any identifiable large shell structure.

WR2 is surrounded by a small, incomplete shell with dimensions $0\rlap{.}'4 \times 0\rlap{.}'3$ on the northern rim of a larger $3\rlap{.}'2 \times 2\rlap{.}'2$ shell, which is likely a superbubble blown collectively by WR2 and other massive stars. The small shell was first reported by Pakull (1991) to be highly ionized, and its abundance was observed by Garnett & Chu (1994). It was later shown that both the small and large shells exhibit He II $\lambda4686$ emission (Nazé et al. 2003). This small shell has an expansion velocity of $\sim$16 km s^{-1} (Chu et al. 1999). On a larger scale, these features are projected on the northwestern rim of H II SGS LMC-7 (Meaburn 1980). There is a known supernova remnant, MCELS J0449-6921 (Maggi et al. 2016), centered $\sim1\rlap{.}'5$ to the northwest of WR2, and it is best seen in the [S II] image. WR2 is more than 100 pc from LH1, thus not likely a member of this OB association.

WR3 is located in a field with a network of faint Hα filaments without obvious shell structure. In the 8 μm and 24 μm images, there is a long, thin filament extending from the eastern vicinity to $1\rlap{.}'6$ north of the star; however, it is uncertain whether this filament is physically associated with WR3. The background H I gas shows two radial velocity components at 282 and 295 km s^{-1}, which may indicate a large-scale expanding structure, but no H I giant shells have been identified. The relationship between the gas kinematics and the WR star is unclear.

WR4 is surrounded by a $0\rlap{.}'6$ shell on the eastern rim of a $4\rlap{.}'3 \times 4'$ shell extending from the luminous H II region DEM L10 around the OB association LH2. The small shell is best seen in the 24 μm image. WR4 is inside H I GS 9, as corroborated by the split velocity components in the H I. The WR star is projected at $\sim$80 pc from LH2, thus not likely a member of this OB association. Details of this object have been reported by Gvaramadze et al. (2014).

WR5 is in a complex network of faint Hα filaments located on the northern rim of H II SGS LMC-7, and some filaments appear to form a large shell measuring $18' \times 12'$ with its major axis oriented along the NE-SW direction. Nei-

ther the shell nature nor the physical association between the star and the shell is certain. WR5 is also projected inside H I GS 9. This H I shell is more extended than the Hα shell in the southeast direction. The star is $\sim$90 pc from LH5, thus not likely a member of this OB association.

WR6 is superposed on diffuse Hα emission in the outskirts of the luminous H II region DEM L22 and associated with the OB association LH5. These features are all on the northern rim of H II SGS LMC-7. The WR star is projected inside H I GS 15, which is corroborated by the H I position-velocity plot. Note, however, that H II SGS LMC-7 is much more extended than H I GS 15.

WR7 is superposed on diffuse Hα emission and projected at $\sim$80 pc from LH5. The 8 μm and 24 μm images show a $4'$ long filamentary arc structure to the west of the star, roughly following the surface of the H I cloud. The infrared arc structure and the apparent H I cavity around the WR star suggest a wind-ISM interaction. The WR star is projected in the interior of H I GS 15 and on the northern rim of H II SGS LMC-7.

WR8 is projected within a faint, filamentary shell-structure with dimensions $11' \times 7\rlap{.}'6$. The [O III] $\lambda5007$/Hα ratio of this shell is higher than other H II regions, indicating a higher excitation. As WR8 is an early type WN3 star with a high effective temperature, it is likely that WR8 has photoionized this nebula.

WR9 is projected in an incomplete, filamentary shell-like structure with dimensions $7\rlap{.}'6 \times 6\rlap{.}'6$ and associated with the OB association LH8. The WR star is also on the western rim of H I GS 18 and inside H II SGS LMC-7. The H I position-velocity plots show split velocity components from the expansion of H I GS 18.

WR10 is located in the northern outskirts of the H II complex N11. The overall morphology of this region suggests an outflow from the prominent central superbubble around LH9, and the H I position-velocity plots show velocity splits indicating expansion. In the Hα image, WR10 is surrounded by a $4' \times 2'$ arc in the north, resembling a half shell, and a straight filament to its west; however, the [O III] image shows that the straight filament is of lower excitation and thus extraneous. The WR star may be partially responsible for the half-shell structure. WR10 is more than 100 pc away from the OB associations LH9 and LH10, thus, it cannot be a member of either.

WR11 is in the prominent $12' \times 8'$ superbubble in the H II complex N11 and a member of the central OB association LH9. The superbubble is inside H I GS 16. The expansion of the superbubble is clearly seen in the H I position-velocity plots.

WR12 is in a $3' \times 2'$ shell in the H II region DEM L39 around the OB association LH12, of which the WR star is a member. This OB association and its H II region are on the northwestern rim of H I SGS 2 and H II SGS LMC-6. The bubble of WR12 was first identified by Chu & Lasker (1980) and has been observed to have an average expansion velocity of 42 km s^{-1} (Chu 1983).

WR13 is located in H I GS 18 and H II SGS LMC-7. The 8 μm and 24 μm images show an arc around the star, which measure $\sim 3\rlap{.}'5$ across. The northeast end of this arc is connected to more emission features. It is difficult to discern whether these features are physically associated with WR13.

WR14 is a known runaway star with a radial velocity of ≤ 130 km s^{-1} relative to the ambient medium (Gvaramadze et al. 2010). There is a $2\rlap{.}'2 \times 1\rlap{.}'4$ bow-shock-like feature northeast of the star, DEM L40; however, the WR star is not at its center of curvature. The H I gas shows two velocity components, although the WR star is not in any catalogued H I shells.

WR15 is surrounded by some complex filamentary features without apparent shell morphology. WR15 is located on the southeastern rim of the N11 complex. The WR star is not in any catalogued OB associations in N11.

WR16 does not show any obvious Hα emission in its vicinity. The WR star is located inside H I SGS 2 and H II SGS LMC-6. Note that the coordinates of this star in Table 1 have been corrected from Neugent et al. (2018).

WR17 is in a small $2' \times 2'$ shell (Dopita et al. 1994) inside a larger $10\rlap{.}'2 \times 8\rlap{.}'4$ superbubble in DEM L45 (Chu & Lasker 1980). The small shell is best seen in the [O III] line because the spectral type of the WR star is WN3, thus, its photoionized gas has high excitation and high [O III] λ5007/Hα ratio.

WR18 has no obvious nebulosity in its vicinity; however, on a larger scale, it is surrounded by a faint shell-like structure with dimensions $20' \times 20'$. The northern part of the shell is brighter and coincides with H I GS 22. The relationship between the optical shell and the H I shell is not clear as the former is twice as extended as the latter. WR18 is projected outside H I GS 22.

WR19 has a small, incomplete elliptical shell surrounding the star with dimensions $0\rlap{.}'7 \times 0\rlap{.}'3$ (Dopita et al. 1994). This shell's nitrogen abundance indicates enrichment by stellar ejecta (Garnett & Chu 1994; Stock et al. 2011), and its observed average expansion velocity is 80 km s^{-1} (Chu et al. 1999). The WR star is also on the northwest outskirts of the H II region DEM L5.

WR20 is in the diffuse emission region DEM L68 adjacent to the bright H II region DEM L67. The [O III] image shows a diffuse large ring with a much higher [O III] λ5007/Hα ratio than the bright H II region DEM L67. The ring measures $7\rlap{.}'7 \times 4\rlap{.}'3$ and might be associated with the WR star. The star is also projected on the periphery of H II SGS LMC-8. The H I

position-velocity plots show velocity splits, but no H I shell was cataloged.

WR21 is inside a $3\rlap{.}'0 \times 2\rlap{.}'8$ shell-like structure in the H II region DEM L66. The WR star is not in known OB associations. WR21 is also projected on the northern rim of H I SGS 5. The H I gas shows two velocity components possibly associated with H I SGS 5.

WR22 has no nearby nebulosity but is located in H II SGS LMC-8. The WR star is over 100 pc away from LH18 and LH26, which is too distant for a membership.

WR23 is surrounded by some faint diffuse and filamentary Hα emission features but with no recognizable shell structures. The WR star is within 50 pc to the rim of LH26 but over 100 pc to its center, thus, it is unlikely to be a member. WR23 is also projected in H II SGS LMC-8.

WR24 is located in a blister-like structure of dimensions $4\rlap{.}'4 \times 3'$ extending from the bright H II region DEM L86 to the west. There are fainter filaments extending to the north and south of this blister structure, but the relationship between them is not clear. DEM L86 is photoionized by the OB association LH31, of which WR24 is a member. The WR star is near the eastern interior of H I SGS 5. The H I gas shows two velocity components possibly associated with the expansion of H I SGS 5.

WR25 is at the base of an east-west elongated shell, measuring $2\rlap{.}'8 \times 1\rlap{.}'4$ and extending from the bright H II region DEM L86 to the east (Dopita et al. 1994). DEM L86 is photoionized by the OB association LH31, of which WR25 is a member. The complex is on the eastern rim of H I SGS 5. The H I gas shows two velocity components possibly associated with the expansion of SGS 5.

WR26 is on the bright southern rim of the $10\rlap{.}'2 \times 7\rlap{.}'4$ shell structure of DEM L105, which is centered on the OB association LH36. However, WR26 is a member of a different OB association, LH37, on the southern rim of DEM L105. There are no sharp filaments near WR26 indicating stellar wind interaction. The whole structure is inside H I GS 44.

WR27 is a member of the OB association LH39 and inside the incomplete shell structure DEM L110 with dimensions $7' \times 4\rlap{.}'6$. It is likely that the OB association is responsible for shaping the shell structure. Interestingly, the 8 μm image shows that WR27 is near the center of an apparent cavity. DEM L110 is inside H I GS 45.

WR28 is superposed on some diffuse Hα emission without any filamentary or shell morphology between the shell H II regions DEM L105 and DEM L106, which are centered on the OB associations LH36 and LH38, respectively. At a distance of $\sim$30–35 pc from each OB association, it is not clear whether the WR star is a field star or a runaway star originating from one of these OB associations. The WR star and the neighboring H II regions DEM L105 and DEM L106 are located inside H I GS 44.

WR29 is inside a 2′.8 × 2′.6 shell structure extending from the bright H II region DEM L108. The shell is better seen in the 8 μm and 24 μm images. The WR star is ∼10 pc from the edge the OB association LH35 and within 50 pc from the center. WR29 is projected within H I GS 46.

WR30 is projected near the eastern interior of the 10′.2 × 7′.4 shell H II region DEM L105 and is located ∼25 pc outside the OB association LH36, which is at the center of DEM L105. The WR star and DEM L105 are inside H I GS 44.

WR31 is in the diffuse H II region DEM L119 with some filaments on the bright southern part of the H II region. The WR star is projected on the southwest rim of H I GS 47.

WR32 is superposed on some diffuse emission to the west of DEM L132a. There are some random filaments nearby but no organized shell structure. The WR star is projected on H I GS 51. The H I gas shows two velocity components associated with the expansion of H I GS 51.

WR33 and WR34 is in a tight cluster in the OB association LH41 and located inside the H II region DEM L132a. The cluster is in H I GS 54.

WR35 is on the edge of the H II region DEM L132b and is a member of the OB association LH41. Due to the large number of massive stars in the vicinity, multiple clusters in LH41, and complexity in the nebula structure, it is not possible to identify specific features associated with the WR star. No small bubbles are seen around the star. The star is projected in H I GS 54.

WR36 is a member of the OB association LH42 and is on the northwest rim of a small 1′.4 × 1′.1 shell structure, though they are likely not associated. The 8 μm image shows a 2′.6 × 2′ cavity around the WR star, and the H I position velocity plots also show a slowly expanding shell structure around the WR star. The WR star could be responsible for excavating this cavity. The bright H II region DEM L143 is associated with the OB association LH42.

WR37 is located in the OB association LH43 and inside the large 13′.8 × 12′.8 superbubble DEM L137 (Chu & Lasker 1980). The superbubble expansion velocity was observed to be 15–20 km s^{-1} (Chu 1982b). The WR star is also projected in H I SGS 6.

WR38, WR 39 are near some nebulosities and are associated with the OB association LH45. These two WR stars are inside H II SGS LMC-5 with complex filamentary structure. No specific structures can be identified to be specifically associated with these WR stars. H II SGS LMC-5 is associated with H I SGS 7.

WR40 is located inside the OB association LH47 on the southwest rim of the superbubble in DEM L152. The WR star is also in the base of a blowout-like structure extending 1′.8 long and 1′.2 wide.

WR41 is in the large elliptical shell DEM L165 of dimensions 8′.1 × 5′.5 with an opening on the southeast quadrant while the south rim of the shell extends from the base of the major axis to the northeast for about 6′ (Chu & Lasker 1980). The expansion velocity of this shell has been determined to be less than 10 km s^{-1} (Chu 1982b). The H I position-velocity plot indicates an expansion with an expansion velocity of ∼12 km s^{-1} . The WR star is not in any known OB associations and is located on the south rim of H I GS 61.

WR42 is in the bright diffuse H II region DEM L160, which has nonuniform surface brightness with dust lanes and emission filaments but does not have any discernable shell structure around the star. The WR star is a member of LH49.

WR43 is inside the 15′.4 × 12′.7 superbubble DEM L164. The superbubble is around the OB association LH50, of which WR43 is a member. DEM L164 is on the south rim of H II SGS LMC-9 and inside H I GS 61. The largest line splitting of the H I position-velocity plot shows an expansion of H I GS 61 of up to 20 km s^{-1} .

WR44 is projected inside the H II SGS LMC-5. Some faint Hα filaments are seen within the central cavity of LMC-5 and together, these filaments are called DEM L154. The filament to the south of the star is curved away from the star, thus, it is unlikely that the WR star is responsible for shaping this feature. The WR star is also inside H I SGS 7.

WR45 is in the H II region DEM L174, which shows striations in its morphology (Chu & Lasker 1980). Although there is an apparent cavity near the star and some curved filaments suggesting wind-ISM interaction, the overall H II morphology does not indicate any shell structure. The internal motion does not indicate an expansion (Chu 1982b). The WR star is projected outside the northwest rim of H II SGS LMC-3.

WR46 is in a small emission nebula with numerous dust lanes to the north of the star. This small nebula is interior to the northern rim of a 7′.6 × 3′.8 shell structure. WR46 is ∼80 pc from the OB association LH52 thus likely not a member of this OB association. The WR star is also projected on the eastern rim of H II SGS LMC-5 and in H I SGS 7.

WR47 is inside the 12 × 9′.5 superbubble DEM L192 and a member of the OB association LH54. DEM L192 is projected on the southwest rim of H II SGS LMC-4 and H I SGS 11. Stock et al. (2011) reported a small nebula around this star and that its elemental abundances are similar to those of LMC H II regions. However, *Hubble Space Telescope* images have resolved this small nebula into bright-rimmed dust globules, and *Spitzer Space Telescope* has revealed embedded star formation (Chu et al. 2005); thus, this nebula has no association with the WR star. These bright-rimmed dust globules can be seen in the MCELS2 Hα image, and the young stellar objects in the dust globules can be seen in the 8 μm and the 24 μm images. The surface of the globules might be photoionized by WR47, but this nebula is not

shaped by the WR star and there is no evidence of wind-ISM interaction.

WR48 is inside a $3.\!'8 \times 2.\!'9$ shell structure in the southeast lobe of DEM L175a while the northwestern lobe is a supernova remnant. Overall, the structure is shaped like a double-lobed nebula and is located in the interaction zone between H II SGS LMC-4 and H II SGS LMC-5 and the interaction zone between H I SGS 7 and SGS 11. The shell's large size, 50 pc across, makes it uncertain whether it is a bubble blown by WR48.

WR49 and WR50 are members of the OB association LH58 in the $10' \times 10'$ superbubble DEM L199, which is on the west rim of H II SGS LMC-3. The WR star is also in H I SGS 12.

WR51 is projected along a curved filament of the H II region DEM L198, which is inside H II SGS LMC-3. The WR star is also in H I SGS 12.

WR52 is member of the OB association LH58 in the $10' \times 10'$ superbubble DEM L199, which is on the west rim of H II SGS LMC-3. A continuum-subtracted [O III]/Hα ratio map reveals a small $0.\!'8 \times 0.\!'8$ shell around the star (Oey et al. 2000). While this small shell is prominent in the [O III]/Hα map, only partial northwestern and southeastern rims of this shell can be seen in the MCELS2 Hα and MCELS1 [O III] images. This small bubble has also been noted by Dopita et al. (1994). The WR star is also in H I SGS 12.

WR53 is in the OB association LH62 and inside the superbubble DEM L208, measuring $14.\!'4 \times 13.\!'5$ and has multiple rings most prominent in the Hα image (Chu & Lasker 1980). DEM L208 is on the northeastern rim of H II SGS LMC-9.

WR54 is superposed on the faint, diffuse H II region DEM L210 with a filamentary shell-like structure, measuring $3' \times 2.\!'4$, extending from the star to the south. DEM L210 is projected inside in H II SGS LMC-3 and H I SGS 12.

WR55 is in the faint diffuse emission region DEM L210 and is a member of the OB association LH61. DEM L210 is projected within H II SGS LMC-3 and H I SGS 12.

WR56 is in the faint diffuse emission region DEM L210 and is $\sim$60 pc from LH61 thus not a member of this OB association. DEM L210 is projected within H II SGS LMC-3 and H I SGS 12.

WR57 is in the faint diffuse emission region DEM L210, which is projected within H II SGS LMC-3 and H I SGS 12.

WR58 is a member of the OB association LH64 and projected on the northern interior of H II SGS LMC-3 and H I SGS 12.

WR59 is projected on the southern interior of H II SGS LMC-3 and H I SGS 12.

WR60 is located near some diffuse nebulosity. The WR star is inside H II SGS LMC-3 and H I SGS 12.

WR61 is surrounded by an apparent bow-shock like feature, measuring $1.\!'4 \times 1.\!'4$, which has been known to emit He IIλ4686 emissions (Niemela et al. 1991). However, the MCELS2 Hα and MCELS1 [O III] images show that the "bow-shock" may not be a coherent structure. The WR star is $\sim$70 pc from LH66 and more than 100 pc from LH69, although it is projected within the $14'' \times 11''$ superbubble DEM L221. The WR star is also projected in H II SGS LMC-9 and H I GS 70. The H I position-velocity plots show split components originating from the expansion of H I GS 70.

WR62 is in a cavity of H II SGS LMC-3 and H I SGS 12 with no nearby nebulosity.

WR63 is $\sim$70 pc from the OB association LH64 and is projected on the northern interior of H II SGS LMC-3 and H I SGS 12.

WR64 is on the southern interior of H II SGS LMC-4 without any obvious nebulosity nearby. The WR star is also projected within H I SGS 11, whose expansion is corroborated by the two velocity components in the H I position-velocity plots.

WR65 is near some filamentary structure within the superbubble DEM L221 and on the southwest rim of H II SGS LMC-9. This WR star is a member of the OB association LH69, which is responsible for shaping the $14' \times 11'$ superbubble DEM L221 and the surrounding H I GS 70.

WR66 is superposed on a filament on the eastern rim of H II SGS LMC-3 and $\geq$100 pc from the OB associations LH74 and LH67 thus not likely a member of either.

WR67 is near some filaments on the eastern rim of H II SGS LMC-3 and $\geq$100 pc from the OB associations LH74 and LH67 thus not likely a member of either. It is interesting to note that WR67 is a very late type WN star (WN11); the bright 24 μm emission indicates a very dense stellar wind. There is a small emission nebula at $15''$ northeast of the WR star, and may consist of material ejected by the star. Spectroscopic observations of the nebular abundance are needed to determine its nature.

WR68 is $\sim$60 pc from LH76, thus likely not a member. The WR star is also projected on the western rim of the $11.\!'5 \times 6.\!'5$ superbubble DEM L229, which is blown by LH76 and on the southern rim of the H II SGS LMC-4.

WR69 is not superposed on any detectable nebulosity but is projected near a faint filament on the southern interior of H II SGS LMC-4 and within H I SGS 11. The WR star is also $\sim$90 pc from LH70 thus likely not a member.

WR70 is located in a dusty, complex environment of the H II region DEM L227 with a large arc northeast of the star, but no shell structure can be claimed to be formed by this WR star. DEM L227 is located on the northern rim of H II SGS LMC-3, associated with H I SGS 12.

WR71 is $\sim$75 pc from the OB association LH76, thus likely not a member. The WR star is inside the small $1.\!'5 \times 1.\!'2$ shell DEM L231 (Chu & Lasker 1980), with an expansion velocity no greater than 18 ± 1 km s^{-1} (Chu 1983).

WR72 is in a diffuse emission field of DEM L224, which contains a collection of random filaments without any shell-like structure. This WR star is not in any known OB association.

WR73, WR74, and WR77 are members of the OB association LH81, which is projected inside the $21' \times 15'$ superbubble DEM L246 within H I GS 73. The H I position-velocity plots show the expansion of H I GS 73.

WR75 is inside a $0\rlap{.}'7 \times 0\rlap{.}'2$ bow shock-like structure embedded in the brightest parts of the filamentary conglomeration of DEM L239. The bow shock structure is best seen in the MCELS2 Hα image. DEM L239 is on the northern rim of H II SGS LMC-4 and H I SGS 11.

WR76 is in a small $1\rlap{.}'5 \times 1\rlap{.}'1$ bubble in DEM L240 on the southeastern edge of H II SGS LMC-4 and H I SGS 11. This shell was first observed by Chu & Lasker (1980), and Cowley et al. (1984) reported the high radial velocity of the star, $\sim$470 km s^{-1}, with respect to the LMC velocity, $\sim$270 km s^{-1}.

WR78 is superposed on the filamentary conglomeration DEM L263. There are no obvious wind interaction features that can be associated with this star.

WR79 is in a $0\rlap{.}'5 \times 0\rlap{.}'3$ ring associated with a small $0\rlap{.}'8$ diameter H II region embedded in a diffuse field within the conglomeration of DEM L263. This ring structure, identified as an oval ring nebula by Dopita et al. (1994) and studied by Stock & Barlow (2010), is best seen in the MCELS2 Hα image. Comparisons between the Hα and [O III] images indicate that this ring nebula has a higher [O III]/Hα emission line ratio than the neighboring H II region; this high excitation is expected from WR79's WN3 spectral type. WR79 is $\sim$90 pc from the rim of LH89 thus likely not a member.

WR80 is a member of the OB association LH87. The star is projected inside the $21' \times 15'$ superbubble DEM L246, which is inside H I GS 73. To the east of the WR star a filamentary shell structure can be seen along the northeast rim of the superbubble DEM L246.

WR81 is projected on the eastern interior of H II SGS LMC-4 and H I SGS 11. The WR star is superposed on diffuse emission with no apparent stellar wind interaction features.

WR82, WR83, WR84, and WR85 are members of LH90 and are projected along the western rim of the $7\rlap{.}'5 \times 5\rlap{.}'2$ superbubble 30 Dor C. The H I giant shell associated with this superbubble is H I GS 75. The H I position-velocity plots show that H I GS75 is more extended than the ionized superbubble.

WR86, WR87, WR89, and WR91 are superposed on faint, diffuse emission between 30 Dor and H II SGS LMC-3 and are members of LH89.

WR88 is superposed on faint, diffuse emission between 30 Dor and H II SGS LMC-3 and is a member of LH85.

WR90 is projected on the eastern interior of H II SGS LMC-4 and H I SGS 11. The WR star is superposed on vey faint diffuse emission with no apparent stellar wind interaction features.

WR92, WR93, WR94, and WR95 are members of LH90 near the center of superbubble 30 Dor C, measuring $7\rlap{.}'5 \times 5\rlap{.}'2$. The H I giant shell associated with this superbubble is H I GS 75, and its expansion velocity assessed from the H I velocity splits is 12–15 km s^{-1}.

WR96 is a member of LH88 and is projected in a supernova remnant in DEM L241.

WR97 has an incomplete shell of radius $0\rlap{.}'75$ that can be seen in the Hα image but shows the highest contrast against the background in the [O III] image. On a larger scale, there appears to be a $6\rlap{.}'6 \times 2\rlap{.}'7$ shell that can be seen in the Hα and [O III], and the MCELS2 Hα image reveals sharp filaments along the shell rim. The filaments on the eastern side of the shell structure appear to be connected with other sharp filaments on the southeast rim of 30 Dor C, forming a large arc structure and making the apparent superbubble structure around WR97 highly uncertain. The WR star is located on the northeastern outskirts of 30 Dor C and is $\sim$45 pc from the OB association LH90 thus likely not a member.

WR98 is a member of LH94 and located in an empty field between filamentary Hα emission features that do not seem to be associated with the WR star or LH94. The H I position-velocity plots show multiple velocity components from the ISM.

WR99 is superposed on a band of Hα emission without any wind interaction features and is a member of LH96. On a larger scale, the WR star is surrounded by a $6\rlap{.}'9 \times 5\rlap{.}'2$ filamentary shell-like structure south of 30 Dor C.

WR100 is just outside the eastern rim of the superbubble 30 Dor C with no associated wind interaction features. The WR star is $\sim$60 pc from LH90 thus likely not a member of this OB association.

WR101 is in a diffuse emission region on the western edge of 30 Dor. No wind interaction features are seen in the vicinity of the star.

WR102 is superposed on some diffuse field emission in DEM L261 and south of 30 Dor B without any wind interaction features. The WR star is a member of LH97.

WR103 and WR104 are in a diffuse emission region on the western edge of 30 Dor and $\sim$25 and $\sim$33 pc from the center of LH99, respectively. No wind interaction features are seen in the vicinity of the stars. The H I position-velocity plots show very complex motions in the ISM.

WR105 is superposed on diffuse emission to the south of 30 Dor B without any wind interaction features and is $\sim$60 pc from the center of LH99. The H I position-velocity plots show at least four velocity components, indicating a very complex interstellar environment.

WR106 is in a small cluster with diffuse field emission on the northern edge of 30 Dor B and a member of LH99. No wind interaction features are seen in the vicinity of the star.

WR107 is in an apparent cavity of dimensions $4\rlap{.}'3 \times 1\rlap{.}'6$. There is enhanced emission around the cavity, but it does not have sharp features indicating wind-ISM interaction. It is not clear whether the WR star is responsible for this structure. The H I position-velocity plots show complex motions in the ISM. The WR star is located in DEM L261 to the south of 30 Dor B and is a member of LH97.

WR108 is superposed on diffuse emission with some unorganized filaments in Shell 3 of 30 Dor (Wang & Helfand 1991). It is ∼70 pc from LH100 and ∼75 pc from LH99 and is not likely a member of either OB association.

WR109 is superposed on diffuse emission on the northeastern part of 30 Dor B without any wind interaction features. It is a member of LH99.

WR110 and WR111 are superposed near some faint diffuse emission in DEM L269 without any wind-ISM interaction features. It is a member of LH101.

WR112 is 20 pc northwest of the R136 cluster inside 30 Dor. The WR star is outside the western rim of a $1\rlap{.}'1 \times 0\rlap{.}'9$ shell.

WR113 and WR114 are projected at 12–15 pc southwest of the R136 cluster in 30 Dor. These WR stars are outside the $2\rlap{.}'5 \times 1\rlap{.}'4$ shell around R136. They are superposed on very bright nebulosities, though no wind-ISM interaction features can be seen.

WR115 is on the outskirts of the R136 cluster, LH100, in the center of 30 Dor and is interior to the western end of a $2\rlap{.}'5 \times 1\rlap{.}'4$ shell.

WR116, WR117, WR121, WR122, WR123, WR124, WR125, WR126, WR127, WR128, WR129, WR130, WR131, and WR132 are in the R136 cluster, or LH100, in the center of 30 Dor. This cluster is interior to the western end of a $2\rlap{.}'5 \times 1\rlap{.}'4$ shell. 30 Dor is in H I GS 78. The H I column densities are so high at the core of 30 Dor that self-absorption occurs, causing the apparent depression in surface brightness.

WR118, WR119, WR120 are at ∼12 pc north of the R136 cluster in 30 Dor, but are still within LH100. They are outside the northern edge of the $2\rlap{.}'5 \times 1\rlap{.}'4$ shell around the R136 cluster and interior to the southern rim of a $1\rlap{.}'1 \times 0\rlap{.}'9$ shell. These three WR stars are projected in the boundary between the two shells and are likely associated with the latter shell.

WR133, WR134 are 80 and 60 pc, respectively, north of the R136 cluster, LH100, in 30 Dor. Both are inside Shell 5 of 30 Dor (Wang & Helfand 1991), measuring $8' \times 4'$.

WR135 is in 30 Dor but is ∼30 pc from the R136 cluster. The WR star is superposed on the edge of a dark cloud. No wind-ISM interaction features can be seen.

WR136 is not in the R136 cluster in the center of 30 Dor but is interior to the eastern end of the same $2\rlap{.}'5 \times 1\rlap{.}'4$ shell around the R136 cluster.

WR137 is superposed on bright diffuse emission in DEM L269 with no obvious wind interaction features associated with the star. The WR star is a member of LH101.

WR138 is superposed on bright emission of 30 Dor and is ∼45 pc from the R136 cluster, LH100. No wind-ISM interaction features can be identified close to the star, and the environment is too complex to unambiguously make any associations.

WR139 is projected just outside the eastern rim of Shell 5 of 30 Dor (Wang & Helfand 1991). It is ∼75 pc from LH100 and thus likely not a member.

WR140 is in the faint diffuse outskirts of 30 Dor, about 330 pc from the R136 cluster. There are some broad filamentary structures in the field, but none are curved around the WR star to indicate wind-ISM interaction.

WR141 is in the bright H II region on the southwest rim of the superbubble in DEM L284, which sits in the ridge of very active star formation on the west rim of H II SGS LMC-2. The surrounding of WR141 is quite dusty, and the apparent shell morphology in the [O III] image is caused by embedded dust lanes. This environment is too complex to identify physical structures unambiguously. The WR star is a member of LH103.

WR142, WR144, WR145 are in the central cavity of the $7\rlap{.}'5 \times 6\rlap{.}'3$ superbubble of DEM L269, which sits in the ridge of very active star formation on the west rim of H II SGS LMC-2, corresponding to H I SGS 19. The WR star is a member of LH104 that is responsible for the superbubble in DEM L269.

WR143 is projected within the $12' \times 8'$ superbubble of DEM L284, which sits in the ridge of very active star formation on the west rim of H II SGS LMC-2. The H I position-velocity plot shows very complex velocity structure. The WR star is a member of LH103.

WR146 is on the northeast rim of the $7\rlap{.}'5 \times 6\rlap{.}'3$ superbubble in DEM L269 and on the western rim of H II SGS LMC-2. The WR star is a member of LH104 which is responsible for the superbubble.

WR147 is outside the superbubble of DEM L269 in the ridge of active star formation on the western base of H II SGS LMC-2. The WR star is ∼60 pc from LH104, and is thus likely not a member of this OB association.

WR148 is to the west of a long north-south oriented filament, out of which a faint $2\rlap{.}'8 \times 1\rlap{.}'8$ arc extends around the WR star, forming a shell structure. The bright long filament actually connects fainter filaments on both ends to form a large $6\rlap{.}'3 \times 4\rlap{.}'5$ shell. The star is located in H II SGS LMC-2, DEM L310, and to the east of 30 Dor. The H I position-velocity plots show multiple velocity components, indicating

complex kinematic structures, rendering the aforementioned apparent shells somewhat uncertain.

WR149 is near the small diffuse H II region DEM L294.

WR150 is projected in the central cavity of H II SGS LMC-2, or DEM L310. There are some filamentary features near the star, but nothing can unambiguously be identified to be associated with the star.

WR151 is at the southern edge of the H II region DEM L309 and projected in the northern interior of a large ionized shell measuring $17' \times 15'$, which is associated with H I GS 94. The WR star is a member of LH116.

WR152 is projected on the northern exterior of the H II region DEM L309 and is $\sim$55 pc from LH116. The WR star is near the northern boundary of the large filamentary ionized shell measuring $17' \times 15'$, which is associated with H I GS 94.

WR153 is superposed on faint diffuse emission of DEM L308 inside a large filamentary ionized shell measuring $17' \times 15'$, which is associated with H I GS 94. The H I position-velocity plots show velocity splits indicating an expansion velocity of $\sim$20 km s^{-1} for H I GS 94. The WR star is over 60 pc from LH116 and thus not likely a member of this OB association.

WR154 is projected in a small $1.\!'8 \times 1.\!'3$ elliptical shell in the western interior of a larger $7.\!'5 \times 5.\!'2$ shell in DEM L315 (Chu & Lasker 1980). The expansion velocity of the small shell has been observed to be $\sim$47 km s^{-1} (Chu 1983). DEM L315 is on the northeastern rim of a large $17' \times 15'$ ionized shell associated with H I GS 94.

REFERENCES

Breysacher, J. 1981, A&AS, 43, 203

Breysacher, J., Azzopardi, M., & Testor, G. 1999, A&AS, 137, 117

Chu, Y.-H. 1981, ApJ, 249, 195

Chu, Y.-H. 1982a, ApJ, 254, 578

Chu, Y.-H. 1982b, ApJ, 255, 79

Chu, Y.-H. 1983, ApJ, 269, 202

Chu, Y.-H. 1988, PASP, 100, 986

Chu, Y.-H. 1997, AJ, 113, 1815

Chu, Y.-H. & Kennicutt, R. C. 1994, ApJ, 425, 720

Chu, Y. H. & Lasker, B. M. 1980, PASP, 92, 730

Chu, Y.-H., Gruendl, R. A., Chen, C.-H. R., et al. 2005, ApJL, 634, L189

Chu, Y.-H. & Treffers, R. R. 1981, ApJ, 249, 586

Chu, Y.-H., Treffers, R. R., & Kwitter, K. B. 1983, ApJS, 53, 937

Chu, Y.-H., Weis, K., & Garnett, D. R. 1999, AJ, 117, 1433

Crowther, P. A., Caballero-Nieves, S. M., Bostroem, K. A., et al. 2016, MNRAS, 458, 624

Crowther, P. A., Schnurr, O., Hirschi, R., et al. 2010, MNRAS, 408, 731

Cowley, A. P., Crampton, D., Hutchings, J. B., et al. 1984, PASP, 96, 968

Danforth, C. W. & Chu, Y.-H. 2001, ApJL, 552, L155

Davies, R. D., Elliott, K. H., & Meaburn, J. 1976, MmRAS, 81, 89

de Koter, A., Heap, S. R., & Hubeny, I. 1997, ApJ, 477, 792

Dopita, M. A., Bell, J. F., Chu, Y.-H., et al. 1994, ApJS, 93, 455

Dwarkadas, V. V. 2007, ApJ, 667, 226

Esteban, C., Vilchez, J. M., Smith, L. J., et al. 1991, A&A, 244, 205

Fazio, G. G., Hora, J. L., Allen, L. E., et al. 2004, ApJS, 154, 10

Fehrenbach, C., Duflot, M., & Acker, A. 1976, A&AS, 24, 379

Gaia Collaboration, Brown, A. G. A., Vallenari, A., et al. 2018, A&A, 616, A1

Garcia-Segura, G., Langer, N., & Mac Low, M.-M. 1996, A&A, 316, 133

Garcia-Segura, G., Mac Low, M.-M., & Langer, N. 1996, A&A, 305, 229

Garnett, D. R. & Chu, Y.-H. 1994, PASP, 106, 626

Gvaramadze, V. V., Kroupa, P., & Pflamm-Altenburg, J. 2010, A&A, 519, A33

Gvaramadze, V. V., Chené, A.-N., Kniazev, A. Y., et al. 2014, MNRAS, 442, 929

Heckathorn, J. N., Bruhweiler, F. C., & Gull, T. R. 1982, ApJ, 252, 230

Henize, K. G. 1956, ApJS, 2, 315

Hughes, J. P. 1987, ApJ, 314, 103

Hughes, J. P., Hayashi, I., & Koyama, K. 1998, ApJ, 505, 732

Hunter, D. A., Shaya, E. J., Holtzman, J. A., et al. 1995, ApJ, 448, 179

Johnson, H. M. & Hogg, D. E. 1965, ApJ, 142, 1033

Kim, S., Dopita, M. A., Staveley-Smith, L., et al. 1999, AJ, 118, 2797

Kim, S., Staveley-Smith, L., Dopita, M. A., et al. 2003, ApJS, 148, 473

Langer, N. 2012, ARA&A, 50, 107

Le Marne, A. E. 1968, MNRAS, 139, 461

Lortet, M. C. & Testor, G. 1984, A&A, 139, 330

Lucke, P. B. & Hodge, P. W. 1970, AJ, 75, 171

Maggi, P., Haberl, F., Kavanagh, P. J., et al. 2016, A&A, 585, A162

Marston, A. P., Chu, Y.-H., & Garcia-Segura, G. 1994, ApJS, 93, 229

Marston, A. P., Yocum, D. R., Garcia-Segura, G., et al. 1994, ApJS, 95, 151

Massey, P. & Hunter, D. A. 1998, ApJ, 493, 180

McCray, R. & Kafatos, M. 1987, ApJ, 317, 190

Meaburn, J. 1980, MNRAS, 192, 365

Meixner, M., Gordon, K. D., Indebetouw, R., et al. 2006, AJ, 132, 2268

Meynet, G., Maeder, A., Georgy, C., et al. 2017, The Lives and Death-Throes of Massive Stars, IAUS 329, 3.

Miller, G. J. & Chu, Y.-H. 1993, ApJS, 85, 137

Nazé, Y., Rauw, G., Manfroid, J., et al. 2003, A&A, 401, L13

Neugent, K. F., Massey, P., & Morrell, N. 2018, ApJ, 863, 181

Niemela, V. S., Heathcote, S. R., & Weller, W. G. 1991, Wolf-rayet Stars and Interrelations with Other Massive Stars in Galaxies, 425

Nugis, T. & Lamers, H. J. G. L. M. 2000, A&A, 360, 227

Oey, M. S., Dopita, M. A., Shields, J. C., et al. 2000, ApJS, 128, 511

Pakull, M. W. 1991, Wolf-Rayet Stars and Interrelations with Other Massive Stars in Galaxies, 143, 391

Pietrzyński, G., Graczyk, D., Gallenne, A., et al. 2019, Nature, 567, 200

Prinja, R. K., Barlow, M. J., & Howarth, I. D. 1990, ApJ, 361, 607

Puls, J., Kudritzki, R.-P., Herrero, A., et al. 1996, A&A, 305, 171

Rieke, G. H., Young, E. T., Engelbracht, C. W., et al. 2004, ApJS, 154, 25

Smith, R. C., & MCELS Team 1999, New Views of the Magellanic Clouds, 28

Solf, J. & Carsenty, U. 1982, A&A, 116, 54

Stock, D. J. & Barlow, M. J. 2010, MNRAS, 409, 1429

Stock, D. J., Barlow, M. J., & Wesson, R. 2011, MNRAS, 418, 2532

Testor, G., Schild, H., & Lortet, M. C. 1993, A&A, 280, 426

Toalá, J. A. & Arthur, S. J. 2011, ApJ, 737, 100

van Loon, J. T., Cioni, M.-R. L., Zijlstra, A. A., et al. 2005, A&A, 438, 273

van Marle, A. J. & Keppens, R. 2012, A&A, 547, A3

Wang, Q. D., Gotthelf, E. V., Chu, Y.-H., et al. 2001, ApJ, 559, 275

Wang, Q. & Helfand, D. J. 1991, ApJ, 370, 541

Weaver, R., McCray, R., Castor, J., et al. 1977, ApJ, 218, 377

Westerlund, B. E. & Smith, L. F. 1964, MNRAS, 128, 311